

TKK Dissertations 142
Espoo 2008

**PASSIVATION OF GaAs SURFACES AND FABRICATION
OF SELF-ASSEMBLED In(Ga)As/GaAs QUANTUM RING
STRUCTURES**

Doctoral Dissertation

Abuduwayiti Aierken



**Helsinki University of Technology
Faculty of Electronics, Communications and Automation
Department of Micro and Nanosciences**

TKK Dissertations 142
Espoo 2008

**PASSIVATION OF GaAs SURFACES AND FABRICATION
OF SELF-ASSEMBLED In(Ga)As/GaAs QUANTUM RING
STRUCTURES**

Doctoral Dissertation

Abuduwayiti Aierken

Dissertation for the degree of Doctor of Science in Technology to be presented with due permission of the Faculty of Electronics, Communications and Automation for public examination and debate in Auditorium AS1 at Helsinki University of Technology (Espoo, Finland) on the 14th of November, 2008, at 12 noon.

**Helsinki University of Technology
Faculty of Electronics, Communications and Automation
Department of Micro and Nanosciences**

**Teknillinen korkeakoulu
Elektroniikan, tietoliikenteen ja automaation tiedekunta
Mikro- ja nanotekniikan laitos**

Distribution:

Helsinki University of Technology
Faculty of Electronics, Communications and Automation
Department of Micro and Nanosciences
P.O. Box 3500 (Tietotie 3)
FI - 02015 TKK
FINLAND
URL: <http://nano.tkk.fi/>
Tel. +358-9-4511
Fax +358-9-451 3128
E-mail: abuduwayiti.aierken@tkk.fi

© 2008 Abuduwayiti Aierken

ISBN 978-951-22-9614-9
ISBN 978-951-22-9615-6 (PDF)
ISSN 1795-2239
ISSN 1795-4584 (PDF)
URL: <http://lib.tkk.fi/Diss/2008/isbn9789512296156/>

TKK-DISS-2523

Multiprint Oy
Espoo 2008



ABSTRACT OF DOCTORAL DISSERTATION		HELSINKI UNIVERSITY OF TECHNOLOGY P. O. BOX 1000, FI-02015 TKK http://www.tkk.fi	
Author Abuduwayiti Aierken			
Name of the dissertation Passivation of GaAs surfaces and fabrication of self-assembled In(Ga)As/GaAs quantum ring structures			
Manuscript submitted 20.05.2008		Manuscript revised 23.09.2008	
Date of the defence 14.11.2008			
<input type="checkbox"/> Monograph		<input checked="" type="checkbox"/> Article dissertation (summary + original articles)	
Faculty		Faculty of Electronics, Communications and Automation	
Department		Department of Micro and Nanosciences	
Field of research		Optoelectronics	
Opponent(s)		Prof. Chris F. McConville	
Supervisor		Docent Markku Sopanen	
Instructor		Dr. Juha Riikonen	
Abstract <p>This work concentrates on two topics: (i) GaAs surface passivation methods using different materials and (ii) formation of InAs islands on GaAs and transformation of InAs islands into quantum rings (QRs). All the samples are fabricated by metalorganic vapor phase epitaxy and characterized by optical spectroscopy and atomic force microscopy.</p> <p>InGaAs/GaAs near-surface quantum well (NSQW) structures were used in the GaAs surface passivation studies because of their sensitivity to surface states. Ultra-thin InP, GaP, GaN layers were grown <i>in-situ</i> on top of the NSQW structure as the passivation layer. As-P and As-N exchange on the GaAs surface were also applied for passivation. In all the passivation methods, the photoluminescence (PL) intensities and carrier lifetimes of the NSQWs were significantly increased. The enhancement factor of the PL intensity was up to two orders of magnitude. The study of time durability of the passivation after keeping the samples for months in air ambient showed that those passivation methods protect the samples against oxidation while the unpassivated samples degrade severely. The passivation effects of these materials were also studied using NSQWs fabricated on (110)-oriented GaAs substrates. The suitability of atomic layer deposited (ALD) titanium nitride layer on GaAs surface as an <i>ex-situ</i> passivation layer was also investigated. Although the enhancement factor of the PL intensity is smaller than that obtained by <i>in-situ</i> methods, smooth surface morphology and notable extension of carrier lifetime were observed in the ALD passivated samples.</p> <p>It is known that island formation is severely suppressed on the GaAs (110) surface. This limitation can be overcome by using a thin strain reducing layer, e.g., an InGaAs layer. Relatively uniform InAs islands with an average areal density of 10^9 cm^{-2} were obtained on GaAs (110) substrate at 400 °C using a thin InGaAs strain reducing layer. Transformation of InAs islands into rings was realized by partially capping the InAs islands and annealing under tertiarybutylarsine flow. Effects of growth conditions on ring evolution were studied by varying the thickness of the partial capping layer, annealing time and annealing temperature. It was concluded that the temperature dependence of the diffusion anisotropy of the indium atoms plays an important role in the ring evolution. The annealing process of the partially capped islands affects significantly the ring shape and the optical properties of the QR structure.</p>			
Keywords MOVPE, epitaxy, GaAs, near-surface QWs, passivation, self-assembly, quantum ring			
ISBN (printed) 978-951-22-9614-9		ISSN (printed) 1795-2239	
ISBN (pdf) 978-951-22-9615-6		ISSN (pdf) 1795-4584	
Language English		Number of pages 54 + 46	
Publisher TKK, Department of Micro and Nanosciences			
Print distribution TKK, Department of Micro and Nanosciences			
<input checked="" type="checkbox"/> The dissertation can be read at http://lib.tkk.fi/Diss/2008/isbn9789512296156/			

Preface

One of the best decisions I have ever made was to come into Finland. During this time period of nearly four years I have been studying and working at one of the most advanced research centers in the semiconductor field and living in a peaceful and friendly country where I can get help without delay inside and outside of the university. Not only my studies but also my life have been fruitful here. I want to express my great gratitude to Professor Harri Lipsanen and Docent Markku Sopanen for giving me the opportunity to come and study in Finland.

The work presented in this thesis has been carried out at the Department of Micro and Nanosciences of Helsinki University of Technology during 2005–2008. I am deeply indebted to Docent Markku Sopanen, the supervisor of this work, for his interest and guidance throughout this work as well as for his help with the manuscripts. I want to especially thank Docent Teppo Hakkarainen for his invaluable advice and preparation of the manuscripts. I also want to thank Dr. Juha Riikonen, Dr. Jaakko Sormunen and Dr. Outi Reentilä for their guidance to MOVPE growth and sample characterization in the beginning. Special thanks are acknowledged to Dr. Marco Mattila for his broad and deep knowledge covering everything. I also want to thank Dr. Hannu Koskenvaara and soon-to-be Dr. Pasi Kostamo for their help on the experimental setups for optical characterization. And last but not least, I would like to thank the personnel of both Nanotechnology and Optoelectronics groups for all the help I have got and for the enjoyable working atmosphere.

This work has been funded by China Scholarship Council and Helsinki University of Technology. Xinjiang Technical Institute of Phys. & Chem., CAS, China and Tekniikan edistämmissäätiö are also acknowledged for their financial support.

My deepest thanks also go to my wife, Gulnar, for her love and continuous support by giving up a lot. Thanks for every happy moment brought by my daughter Kitty and born-in-Finland son Azhar. Every smile and kiss from you is a great force pushing me forward.

Finally, I would like to say: *Kiitos Suomi.*

Espoo, May 2008

Abuduwayiti Aierken

Contents

Preface	v
Contents	vi
List of publications	vii
Author's contribution	viii
1 Introduction	1
2 Fundamentals of III-V semiconductors	3
2.1 III-V compound semiconductors and fabrication	3
2.2 GaAs surface passivation	6
2.3 Self-assembled quantum ring structures	8
3 Experimental methods	11
3.1 Metalorganic vapor phase epitaxy	11
3.2 Atomic layer deposition	13
3.3 Atomic force microscopy	14
3.4 Optical spectroscopy	14
4 GaAs surface passivation	19
4.1 In-situ epitaxial passivation of GaAs (100)	19
4.2 Growth on and surface passivation of GaAs (110)	23
4.3 Ex-situ passivation with titanium nitride	27
5 Self-assembled InAs/GaAs quantum ring structures	29
5.1 Self-assembled InAs island formation on GaAs (110)	29
5.2 Transformation of InAs islands into quantum rings	33
6 Summary	38

List of publications

This thesis consists of an overview and of the following publications which are referred to in the text by their Roman numerals.

- I** A. Aierken, J. Riikonen, J. Sormunen, M. Sopanen, and H. Lipsanen, *Comparison of epitaxial thin layer GaN and InP passivations on InGaAs/GaAs near-surface quantum wells*, Applied Physics Letter **88** 221112 (2006)
- II** A. Aierken, J. Riikonen, M. Mattila, T. Hakkarainen, M. Sopanen, H. Lipsanen, *GaAs surface passivation by ultra-thin epitaxial GaP layer and surface As-P exchange*, Applied Surface Science **253** 6232 (2007)
- III** A. Aierken, T. Hakkarainen, J. Tiilikainen, M. Mattila, J. Riikonen, M. Sopanen, H. Lipsanen, *Growth and surface passivation of near-surface InGaAs quantum wells on GaAs (110)*, Journal of Crystal Growth **309** 18 (2007)
- IV** M. Bosund, A. Aierken, J. Tiilikainen, T. Hakkarainen, H. Lipsanen, *Passivation of GaAs surface by atomic-layer-deposited titanium nitride*, Applied Surface Science, **254** 5385 (2008)
- V** A. Aierken, T. Hakkarainen, M. Sopanen, J. Riikonen, J. Sormunen, M. Mattila, H. Lipsanen, *Self-assembled InAs island formation on GaAs (110) by metalorganic vapor phase epitaxy*, Applied Surface Science **254** 2072 (2008)
- VI** A. Aierken, T. Hakkarainen, J. Riikonen, M. Sopanen, *Transformation of InAs islands to quantum ring structures by metalorganic vapor phase epitaxy*, Nanotechnology, **19** 245304 (2008)

Author's contribution

The sample structures and the experimental procedures for all the publications were planned by the author and the co-authors. Sample fabrication for all the publications was carried out by the author. For publication IV, atomic-layer-deposition growth of TiN and its characterization by x-ray reflectivity measurement were done by M. Bosund. Morphological, structural and optical characterization of the samples for all the publications were performed by the author. The manuscripts for all the publications, except publication IV, were written by the author.

1 Introduction

The invention of the semiconductor transistor is one of the greatest scientific events in the twentieth century. Since then, during the past over half a century, semiconductor technology has developed rapidly and has been widely applied in almost every aspect of human life. Semiconductor based high technology has made an enormous contribution to the society and has brought convenient and efficient solutions to people's daily complications. Nowadays it is hard to imagine how the life would be like without semiconductors.

Silicon was the first and is the most widely used semiconductor material for microelectronics involving integrated circuits. Silicon is highly abundant in earth's crust and the advanced silicon industry manufactures silicon based devices at very low prices. However, the main drawback of silicon is that it is an indirect bandgap material and, subsequently, has poor light emitting properties.

GaAs and other III-V compound semiconductors have showed their superiority over silicon in optoelectronic applications. However, the performance of GaAs based materials and devices is partially limited due to the high density of surface states, especially in low-dimensional systems. The surface states pin the Fermi level in the middle of the bandgap and, consequently, lead to high surface recombination rate which not only limits the performance but also reduces the lifetime of devices. Different surface passivation methods have been developed for suppressing this adverse effect. Various *in-situ* and *ex-situ* passivation techniques using different material combinations and processing methods have been intensively investigated for GaAs surface passivation. Improvement of device performance by surface passivation has been reported. Among of them, the epitaxial *in-situ* surface passivation has been shown to be one of the most efficient ways to lower the density of the surface states. Significant enhancement of optical properties can be obtained in passivated samples.

Low dimensional quantum structures, such as quantum well (QW), quantum wire (QWR) and quantum dot (QD) structures, have proved to be very useful in optoelectronic applications, for example, in the semiconductor laser. Besides, ring shaped quantum structures, or quantum rings (QRs), have become a promising candidate for developing novel devices due to their unique electrical, optical and magnetic properties. Some potential applications of QRs and various fabrication techniques of QRs with different materials have been reported. The high lattice mismatch

of InAs/GaAs system enables the formation of well distributed InAs islands by Stranski-Krastanow growth mode. Transformation of these islands into QRs can be carried out by using a thin partial capping layer followed by an annealing at an elevated temperature. This is one of the most direct and efficient ways to fabricate self-assembled semiconductor QRs.

In this thesis, GaAs surface passivation is studied by using *in-situ* and *ex-situ* grown thin layers with various materials to suppress surface effects. Formation of three-dimensional InAs islands and transformation of InAs islands into ring-shaped quantum structures is also investigated. Metalorganic vapor phase epitaxy (MOVPE) is used for sample fabrication. Passivation effects are characterized by probing the optical properties of the passivated samples and comparing them to those of the unpassivated reference samples. Surface morphology of passivated samples and properties of InAs islands and quantum ring structures are studied by atomic force microscopy (AFM).

The structure of this overview is as follows. In chapter 2, a brief introduction of III-V semiconductors, GaAs surface passivation and self-assembled quantum ring structures are presented. The main experimental methods used in this work, i.e., MOVPE, AFM, and optical spectroscopy are introduced in Chapter 3. The results reported in publications I–IV are presented in chapter 4 which discusses the GaAs surface passivation by *in-situ* and *ex-situ* grown layers. The results from publications V–VI, InAs island formation on GaAs and evolution of these islands into rings, are presented in chapter 5. The main results of this thesis are summarized in chapter 6.

2 Fundamentals of III-V semiconductors

In this chapter, a brief introduction to III-V compound semiconductors and epitaxial growth is presented. The fundamentals of GaAs surface passivation and self-assembled quantum ring structures are also reviewed.

2.1 III-V compound semiconductors and fabrication

Although the elemental semiconductors, in particularly silicon, have been very useful for the development of microelectronics, they have some important drawbacks. The bandgaps of these semiconductors are indirect, which implies that their light emitting and absorption coefficients are low. For optoelectronic applications it was natural to look for other materials. It turned out that compound semiconductors, particularly III-V compounds, offered many of the desired properties and could be synthesized without much difficulty [1].

Two important events, the invention of the semiconductor laser [2] and the discovery of the Gunn effect [3], turned more and more interests into III-V compounds such as GaAs and InP. Compared to Si and Ge, GaAs and InP have high electron mobilities which is an important property for the development of high-speed electronic devices. Their direct bandgaps and the consequent high radiative efficiencies make them important as optoelectronic materials. Another important III-V compound material is GaP, which has its bandgap in the visible part of the spectrum and, therefore, is suitable for light-emitting-diode (LED) devices [4, 5]. Recently, research on GaN [6, 7] and other III-nitride compounds [8, 9] has also showed the potential of these materials in LED applications.

Another attractive feature of the binary III-V compounds is that they can be combined or alloyed to form ternary or quaternary compounds. Therefore, it is possible to vary the bandgap, and, subsequently, the electronic and optical properties. Fig. 2.1 shows the bandgap energies and lattice constants of various III-V compound semiconductors. The ternary compounds are indicated by the lines between the binary compounds. The energy bandgaps of these III-V compounds vary in a wide range and the corresponding photon wavelengths cover the spectrum from infrared to ultraviolet. The "bandgap tailoring" by formation of ternary and qua-

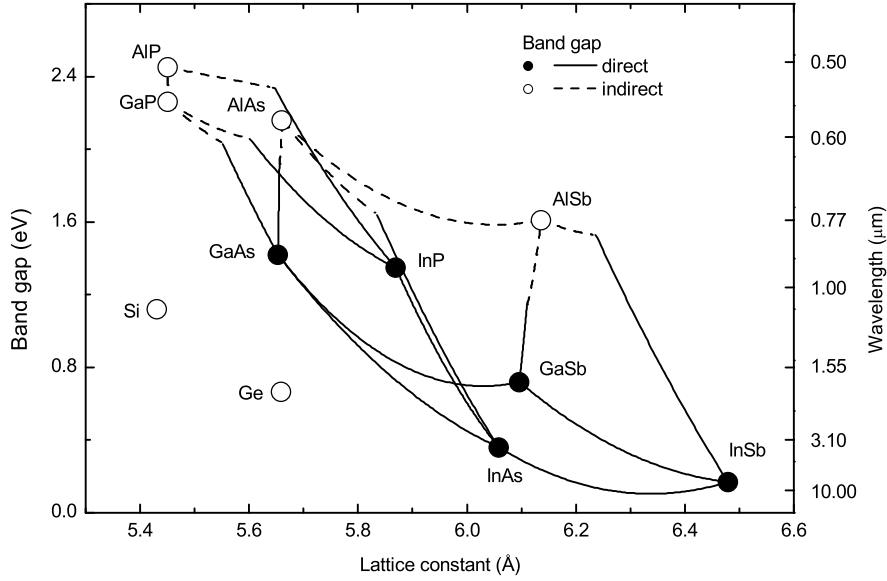


Figure 2.1: Bandgap energy and lattice constant of various III-V semiconductors. [10]

ternary compounds also enables the formation of heterojunctions, which have become essential for the design of high-performance electronic and optical devices. For example, InAsSb-based mid-infrared lasers [11], infrared photodiodes using the InAs/Ga_{1-x}In_xSb superlattice [12] and high-power ultra-violet InGaN/AlGaIn double-heterostructure LEDs [13] have been reported.

Fabrication of III-V heterostructures is carried out commonly by epitaxial growth techniques such as metalorganic vapor phase epitaxy (MOVPE) and molecular beam epitaxy (MBE). Epitaxy or epitaxial growth is the process of growing a crystal of a particular orientation on top of another crystal, where the orientation is determined by the underlying crystal, the substrate. In homoepitaxy the grown layers are made up of the same material as the substrate, while in heteroepitaxy the grown layers are of a material different from the substrate. One of the most crucial problems related to heteroepitaxy is the lattice mismatch, or misfit, between the substrate and the epilayer. Because the substrate is usually much thicker than the epilayer, the crystalline structure of the epilayer can be maintained only if the epilayer is elastically strained. If the strain is incorporated into the epilayer coherently, the lattice constant of the epilayer is forced to be equal to the lattice constant of the substrate in horizontal directions and is forced to expand or shrink in the crystal growth direction. After a certain critical thickness, the elastic energy can be released through dislocation formation or partially relaxed by formation of islands.

Three fundamental growth modes in heteroepitaxy associated with initial nucleation and growth of the epi-layer have been identified. These three modes, Frank-van der Merwe (F-M) [14], Volmer-Weber (V-W) [15], and Stranski-Krastanow (S-K) [16],

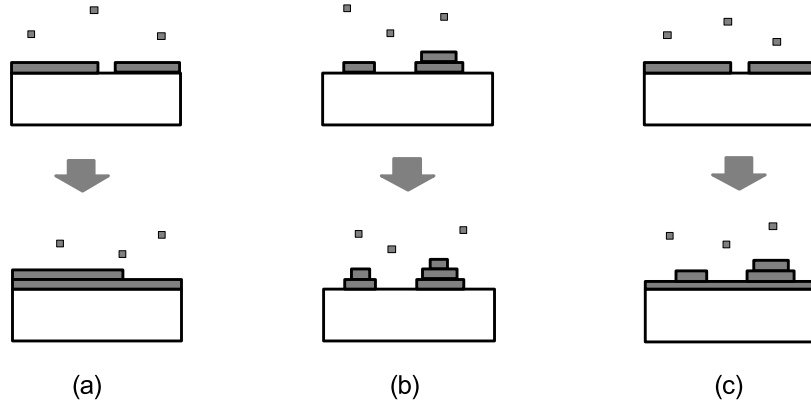


Figure 2.2: Three basic growth modes in heteroepitaxy: (a) Frank-van der Merwe (b) Volmer-Weber (c) Stranski-Krastanow.

are shown schematically in Fig. 2.2. The F-M mode (layer-by-layer growth) can be observed when the chemical bonding and lattice parameters are close to each other between the two materials. In this growth mode, the lattice mismatch is very small and adatoms are more strongly bonded to the substrate than to each other. The V-W mode (island growth), on the other hand, occurs when the adatoms are more strongly bonded to each other than to the substrate. This mode is typical for highly mismatched and dissimilar materials.

There is an intermediate case, S-K mode (layer plus island growth), between the F-M and V-W modes. At the beginning of the growth the epitaxial layer grows pseudomorphically on the lattice-mismatched substrate and the strain energy increases linearly with the thickness of the grown layer. When the thickness exceeds a critical thickness, the strain energy is released through dislocation formation. Another route for partial relaxation is the formation of islands. In S-K mode, a very thin, typically few monolayers, two-dimensional wetting layer is formed first then three-dimensional islands are formed on top of the wetting layer. The driving force for island formation is the minimization of the strain energy of both the epilayer and the substrate. When the strain relaxation occurs only by island formation without dislocation, it is called coherent S-K mode, first reported on Ge island growth on silicon substrate [17]. In coherent S-K mode, the lattice mismatch is partially accommodated around the island and the strain energy is partially relaxed by the deformation of the substrate in some range. Three-dimensional island growth by coherent S-K mode have been studied in different material systems, such as, InGaAs/GaAs [18], InAs/GaAs [19], InGaAs/AlGaAs [20], InP/GaAs [21], InAs/InP [22], and GaSb/GaAs [23]. The island formation not only changes the morphological structure, but also affects the energy states of the system. By covering the islands with a thick barrier layer having higher bandgap energy than the island material, carriers can be confined in all three directions so that a set of discrete energy states is induced. In this case, the islands are called quantum dots.

2.2 GaAs surface passivation

As described in the previous section, the GaAs based III-V compound semiconductors have promising advantages over silicon in optoelectronic applications. However, the performance of GaAs based materials and devices is partially limited due to the high density of surface states. This is especially evident in low-dimensional systems located near or at the surface. The lack of control of the surface and interfaces has exerted some limitation on the broader use of these materials.

At a semiconductor surface, the crystal periodicity is interrupted and the chemical bonds are broken. The surface is chemically and electrically more active due to these "dangling bonds". Clean semiconductor surfaces in vacuum typically minimize the bond and strain energies by surface relaxation or surface reconstruction. This reorganization of surface atoms provides electronic states which are different from those in the bulk. When these states have their energy levels around the middle of the bandgap, the charge carriers can be "trapped" at the surface. Additionally, the surface states pin the Fermi level around the middle of the bandgap and lead to band bending at the surface. This phenomenon is called Fermi level pinning [24–28] and is illustrated in Fig. 2.3. Fermi level pinning not only happens on clean semiconductor surfaces in vacuum, but also on insulator-semiconductor or metal-insulator-semiconductor interfaces. In these cases, surface traps are created from lattice mismatch defects or interface states in the bandgap.

When a clean semiconductor surface is exposed to air ambient, a thin oxide layer is typically formed on the surface and also leads to Fermi level pinning. For example, the Fermi energy gets pinned at approximately 0.75 eV and 0.52 eV above the valence band maximum in n-type and p-type GaAs, respectively, because of the native oxides. [28]. The presence of a large number of electronically active surface states results in a reduced device performance and reliability. The effects of these states manifest themselves in a variety of different ways, and they adversely affect a majority of devices. For example, in heterojunction bipolar transistors (HBTs), the defects may cause a high rate of recombination along the mesa surfaces, resulting in lower current gain; in photodiodes, they may cause large reverse leakage currents, lower breakdown voltage, and lower responsiveness.

The technology of reducing this adverse effect of semiconductor surface states is referred to as passivation. The passivation effects can be achieved by either replacing the active surface (arsenic atoms in GaAs) with less chemically active atoms (such as sulphur, phosphor and nitrogen etc. for GaAs) or cover the surface with a material having lower surface state density and lower oxidation rate. Developing a proper and effective passivation technique requires a good understanding of the nature of the states and causes of their origin. Unfortunately, the fundamental knowledge of the semiconductor surfaces has been limited due to the enormous complexity of the surface both in terms of its structure and electrical properties. Therefore, the

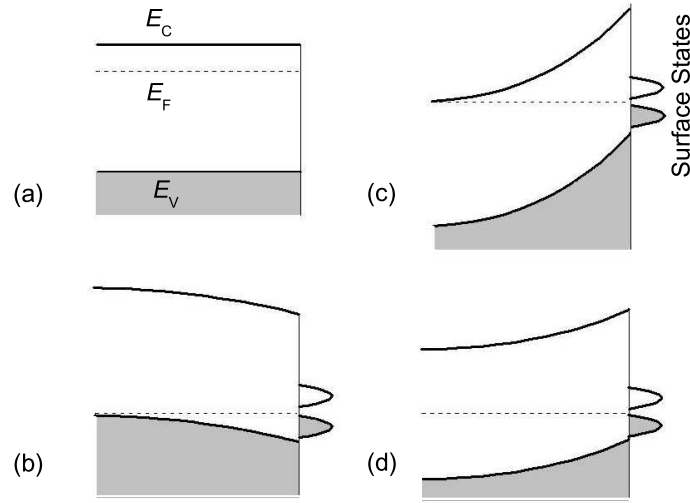


Figure 2.3: Schematic diagram of surface band bending and surface states in semiconductor. (a) n -type semiconductor without Fermi level (E_F) pinning, (b) p -type semiconductor with E_F pinning, (c) n -type semiconductor with E_F pinning, and (d) near-intrinsic semiconductors with E_F pinning close to the valence band. [27]

research on passivation technology has been mainly based on empirical techniques [28].

Various *in-situ* and *ex-situ* passivation techniques using different material combinations and processing methods have been intensively investigated for GaAs surface passivation. Improvement of device performance by surface passivation has been reported [29–32]. Chemical passivation with sulphur [33–36] and surface phosphorization by As-P exchange methods [37–40] are the most widely studied conventional passivation methods. The sulphur treatment of the GaAs surface in sulphide solutions results in the removal of the native oxide layer by formation of As-S and Ga-S covalent bonds. These processes are accompanied by a marked reduction of the surface recombination velocity which is indicated by an enhancement of photoluminescence of sulphur treated GaAs. In surface phosphorization of GaAs, a thin GaP layer is formed via exchange of As and P atoms on the surface. GaP has one of the lowest oxidation rates amongst the III-V compounds and has a more stable surface structure than GaAs, so it will protect the GaAs surface from oxidation. Furthermore, group III-phosphides are characterized by a lower density of surface states than III-arsenides and, therefore, a lower density of electronic traps is expected on the surface [41, 42].

Variety of plasma nitridation methods [43, 44], chemical treatment [45, 46], and protective layer deposition by hydrogen [32, 47], silicon nitride [48, 49] or oxides [50, 51] also have been demonstrated to passivate the GaAs surface. Besides, more and

more new materials and techniques [52, 53] for surface passivation are emerging along with the rapid development of nanotechnology. However, epitaxial *in-situ* surface passivation has been shown to be the most efficient way to reduce the surface state density [54–56]. Significant passivation effects can be achieved by, e.g., MOVPE grown thin InP and GaN layers. The PL intensity of passivated near surface QWs have been reported to increase by a factor of more than 10^4 [55].

The *in-situ* and *ex-situ* passivation techniques can be applied based on the demand and material availability. In *in-situ* methods, the passivation takes place right after the sample growth in the reactor so that the passivation layer can be grown on oxide-free "fresh" surface and achieve the best passivation effect. However, the limited types of precursors on MOVPE or MBE systems prevent the usage of various materials in passivation. The *ex-situ* passivation, on the other hand, has the advantages of low process temperature, a variety of passivation materials, and applicability on both flat surfaces and processed devices. But the surface oxides should be removed before the passivation process. Typically, the oxide removal is carried out by a chemical treatment of the surface, i.e. by etching with acids, which probably induce more defects to the surface and really cannot remove all of the native oxides formed after the GaAs surface is exposed to air.

2.3 Self-assembled quantum ring structures

When a narrow-bandgap material is completely surrounded by a larger bandgap material, the electrons and holes are confined into discrete quantum states and their movement is restricted in one, two, or three dimensions depending on the structure. These kind of structures are known as quantum well (QW), quantum wire (QWR), and quantum dot (QD) structures, respectively. A QW structure is obtained by growing a flat narrow-bandgap material layer between layers of larger bandgap materials resulting in carrier confinement in the crystal growth direction. The QWR structure, in which the carriers are confined in two dimensions, can be obtained by selective growth on striped surfaces or by forming stripes via chemical etching. The QD structure, on the other hand, can be fabricated by enclosing, e.g., 3D islands within a larger bandgap material. All of these quantum structures have been studied intensively and have achieved great applications in optoelectronic and microelectronic fields.

However, due to their ring-like geometric shape, QR structures have unique electrical [58–60], optical [60, 61] and magnetic [62–64] properties different from those of the conventional quantum structures. It has been shown experimentally that QRs can confine carriers into ring like quantum states [65]. By stacking layers of self-assembled rings, a QR laser structure has been fabricated [66]. When a QR is placed in a perpendicular magnetic field, a phase shift of electron wave function proportional to the flux has been reported (known as Aharonov-Bohm effect [67]).

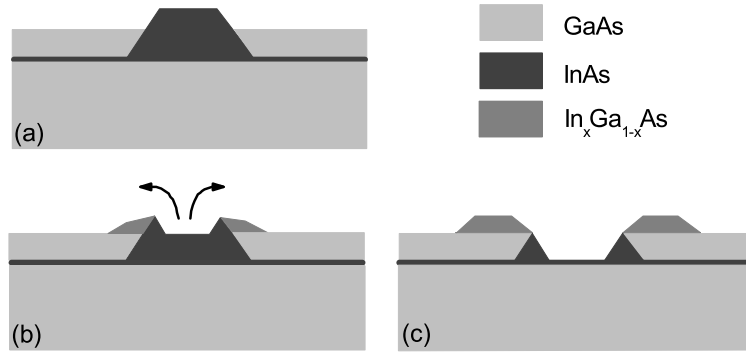


Figure 2.4: Schematic diagram of the kinetic model of the formation of In(Ga)As QRs by partially capping an InAs island. (a) The island partially capped by GaAs, (b) mobile indium atoms diffuse outward, and (c) a void left in the middle of the initial island. [57]

Besides, the experimental observation of persistent currents [68] in QR structures has brought more theoretical and experimental interest [69, 70] to this field. These electronic and magnetic properties of the QR structure make QRs a promising candidate for developing novel devices.

In addition to studies on electronic properties of QRs, the fabrication techniques of QRs have attracted a lot of attention. The self-assembled growth of semiconductor QRs was carried out first by García *et al.* in an MBE system by covering InAs islands with a GaAs capping layer [71]. Since then numerous theoretical and experimental studies of QRs have been reported. Although In(Ga)As/GaAs [72–74] is by far the most studied of the QR structures, other types of growth techniques and materials have also been applied to the fabrication of QRs. For instance, it was observed that growing an additional AlAs layer on top of the GaAs partial capping layer enhances the InGaAs QRs formation by reducing the surface diffusion of gallium atoms [75]. A thin InP partial capping layer, instead of the conventional GaAs layer, was used to ring transformation of InAs islands on an InP substrate [76]. GaSb/GaAs QRs were formed by controlling the thickness of the GaSb layer grown on GaAs without partial capping layer followed by annealing [77]. Additionally, InAs/InP QR formation by As-P exchange without partial capping layer [78, 79] and direct formation of InGaAs/GaAs QRs by annealing Ga droplets under As flow [80] have also been demonstrated. A latest research report [81] shows that the quantum ring structure also can be obtained by selective wet etching buried In(Ga)As dots.

The possible mechanism of island-to-ring evolution in In(Ga)As/GaAs system has been studied intensively [82–84] and two different models have been suggested to explain the transformation process. It has been concluded that the overgrowth of InAs islands with GaAs is a non-equilibrium process. The partial capping layer does

not cover the islands because the strain makes the apexes of the islands unfavorable locations for GaAs growth, i.e., the island apexes remain uncovered [82].

The kinetic model is based on the different surface diffusion rates of group III atoms. Indium atoms are more mobile at typical annealing temperatures and gallium atoms, on the other hand, experience only limited diffusion after they have been incorporated into the crystal lattice. Consequently, the indium atoms on top of an InAs island diffuse outward and a ring shaped (In-Ga)As alloy rim with a void in the center of the initial island will be formed, as shown in Fig 2.4. Due to the larger diffusion constant of In atoms along $[1\bar{1}0]$ than $[110]$ direction [83], the QRs are not completely circular but elongated in $[110]$ direction.

The thermodynamic model, on the other hand, suggests that the partial capping layer induces a change in the balance of surface free energy and, consequently, an outward pointing force is created [82, 84]. As a result, system finds a new equilibrium in a ring structure via material redistribution. However, it has been concluded that the island-to-ring transformation is promoted by both kinetic and thermodynamic mechanisms [82].

3 Experimental methods

The experimental fabrication and characterization methods used in this thesis are introduced in this chapter.

3.1 Metalorganic vapor phase epitaxy

MOVPE, also known as MOCVD (metalorganic chemical vapor deposition), is a chemical vapour deposition method for epitaxial growth of materials, especially compound semiconductors from the surface reaction of organic compounds or metalorganics and hydrides containing the required chemical elements [85]. In the MOVPE process the source materials are mixed with a carrier gas and transported into a reactor where the substrate is located on a heated susceptor. When the metalorganic precursor molecules decompose in the hot zone over the substrate, the group III and V elements diffuse to the surface of the substrate. After the atoms are adsorbed to the surface, they can diffuse on the surface, nucleate into the growing epilayer or desorb away (Fig. 3.1). The most attractive features of the MOVPE method are the wide range of metalorganic compounds available as precursors and facility of fabricating highly homogeneous layers, atomically flat surfaces, and sharp material interfaces while controlling the composition precisely.

The samples studied in this thesis were fabricated in a MOVPE system manufactured by Thomas Swan Scientific Equipment Ltd. The schematic diagram of the MOVPE system is shown in Fig. 3.2. All the group-III and group-V source materials are metalorganic compounds. Trimethylindium (TMIn), trimethylgallium (TMGa), tertiarybutylarsine (TBAs), tertiarybutylphosphine (TBP) and dimethylhydrazine (DMHy) are used as sources of indium, gallium, arsenic, phosphorus and nitrogen, respectively. The source materials are held in steel bubblers and kept in temperature-controlled baths. Hydrogen is used as the carrier gas. When the carrier gas flows through the bubblers, it is saturated with the vaporized source material molecules. The concentration of the precursor in the gas is determined by the vapor pressure of the compound at the bath temperature. The flow rate is controlled by mass flow controllers (MFCs). The saturated flow from each bubbler is directed either to the vent line or to the mixing manifolds which lead to the reactor. Separate mixing manifolds are used for group-III and group-V precursors to prevent

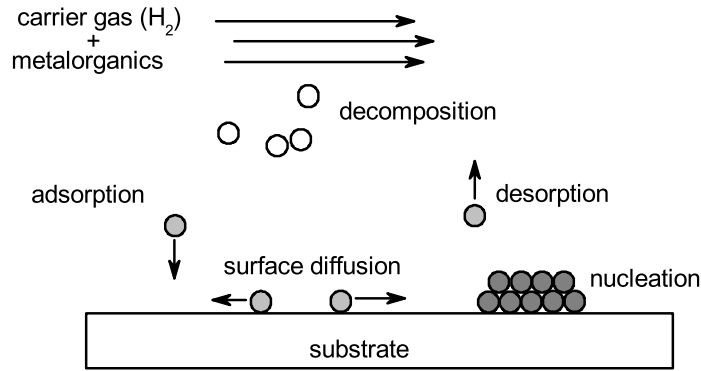


Figure 3.1: Surface processes during MOVPE growth.

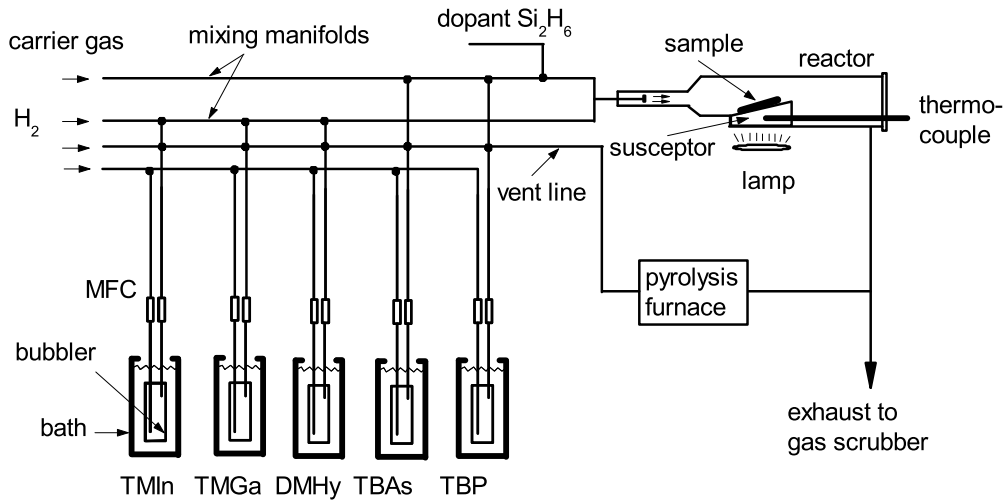


Figure 3.2: Schematic diagram of the MOVPE system.

unwanted pre-reactions before the reactor. The vent line is used for stabilizing the flow rates and the concentrations before the epitaxial growth and to flush the residual materials after the growth. The gas flows from the reactor and the vent line are directed to the exhaust where the toxic particles are absorbed and oxidized in a gas scrubber.

Epitaxial growth takes place in a horizontal quartz-glass reactor at atmospheric pressure. The substrate is placed on a $2 \times 2 \text{ cm}^2$ graphite susceptor which is heated by a halogen lamp located outside of the reactor. The temperature is measured by a thermocouple located inside the susceptor. Due to the cooling effect of the gas flow through the reactor, the actual temperature at the sample surface is approximately $50 \text{ }^\circ\text{C}$ lower than the thermocouple reading at $650 \text{ }^\circ\text{C}$ [86]. All the temperatures mentioned in this thesis are thermocouple readings.

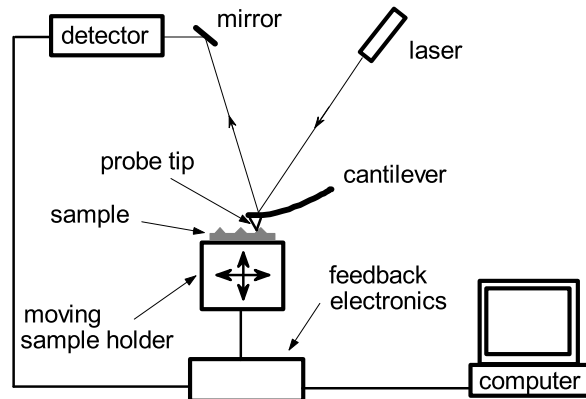


Figure 3.3: Schematic diagram of the AFM measurement.

All the samples studied in this thesis were grown on semi-insulating GaAs (100) or (110) substrates. Prior to the growth process, the substrates were annealed at 700 °C to remove the native surface oxide. Growth temperature, growth rate and other parameters were varied depending on the sample structure. Detailed information about the growth procedures can be found in sections 4 and 5 in this thesis and in the corresponding publications.

3.2 Atomic layer deposition

Atomic Layer Deposition (ALD) is a special case of the chemical vapor deposition (CVD) method [87]. Very good overviews of applications of the ALD technique on semiconductors have been published [88, 89]. It differs from the other CVD techniques by keeping the precursors strictly separated from each other in the gas phase. ALD can be defined as a film deposition technique that is based on the sequential use of self-terminating gas-solid reactions. The growth of material layers by ALD consists of repeating the following characteristic four steps: (1) a self-terminating reaction of the first reactant, (2) a purge or evacuation to remove the nonreacted reactants and the gaseous reaction by-products, (3) a self-terminating reaction of the second reactant, and (4) a purge or evacuation. Steps 1 – 4 constitute a reaction cycle. Each reaction cycle adds a given amount of material to the surface, referred to as the growth per cycle. To grow a material layer, reaction cycles are repeated until the desired amount of material has been deposited.

The main advantages of the ALD are [89]: (i) accurate and simple thickness control by growth per cycle, (ii) no need to control the reactant flux homogeneity, (iii) large area uniformity, (iv) excellent conformality, and (v) low processing temperature when the precursor chemistry is suitably selected. These advantages enable growth

of various materials such as III-V semiconductors, II-VI semiconductors, oxides and nitrides including titanium nitride (TiN) which is often used as a coating to improve various surface properties.

3.3 Atomic force microscopy

Atomic force microscopy (AFM) is a form of scanning probe microscopy, in which the surface morphology is characterized with a probe with the resolution of nanometer scale [90]. It is a versatile tool for studying the surface topology since no special sample preparation is needed and the measurement can be conducted at room temperature in air ambient.

Fig. 3.3 shows a schematic illustration of operating principle of an AFM system. A probe tip is mounted on the end of a triangular cantilever arm, an analog to a diamond stylus mounted on the end of a record player arm. A piezoelectric actuator raster scans the sample beneath the probe tip in lateral directions. As the probe tip undergoes attractive or repulsive forces, the cantilever bends. This bending of the cantilever can be monitored by a reflected laser beam from the back of the cantilever onto a position sensitive photodiode detector. A vertical piezoelectric actuator keeps the sample at a constant distance from the cantilever probe by a correction feedback signal from the detector and, thus, keeps the reflected laser beam at a constant point on the detector. The feedback signal is recorded by a computer as the height information of the surface morphology and an image of the surface features is generated.

A contact-mode NanoScope E AFM was used to characterize the surface morphology of the samples in this work. The maximum scanning area is $13 \times 13 \mu\text{m}^2$ and the probe tips are non-conductive silicon nitride tips with a diameter of 20 nm. The vertical resolution is sufficient (0.1 nm) to observe the atomic layer terraces of the thin passivation layers. The areal density, size and the cross-sectional profiles of the self-assembled InAs islands and rings are calculated from the AFM scanning data.

3.4 Optical spectroscopy

The measurement of the optical properties of the samples is an important part of the research of III-V semiconductor structures in most of the cases. In this thesis, comparison of the optical properties of the passivated and unpassivated samples were used as a key criteria for the effectiveness of passivation. Properties of self-assembled islands and QRs were also studied by optical characterization. Photoluminescence (PL) spectroscopy, time-resolved photoluminescence (TRPL) and photoreflectance (PR) spectroscopy were utilized to study the optical properties of the samples.

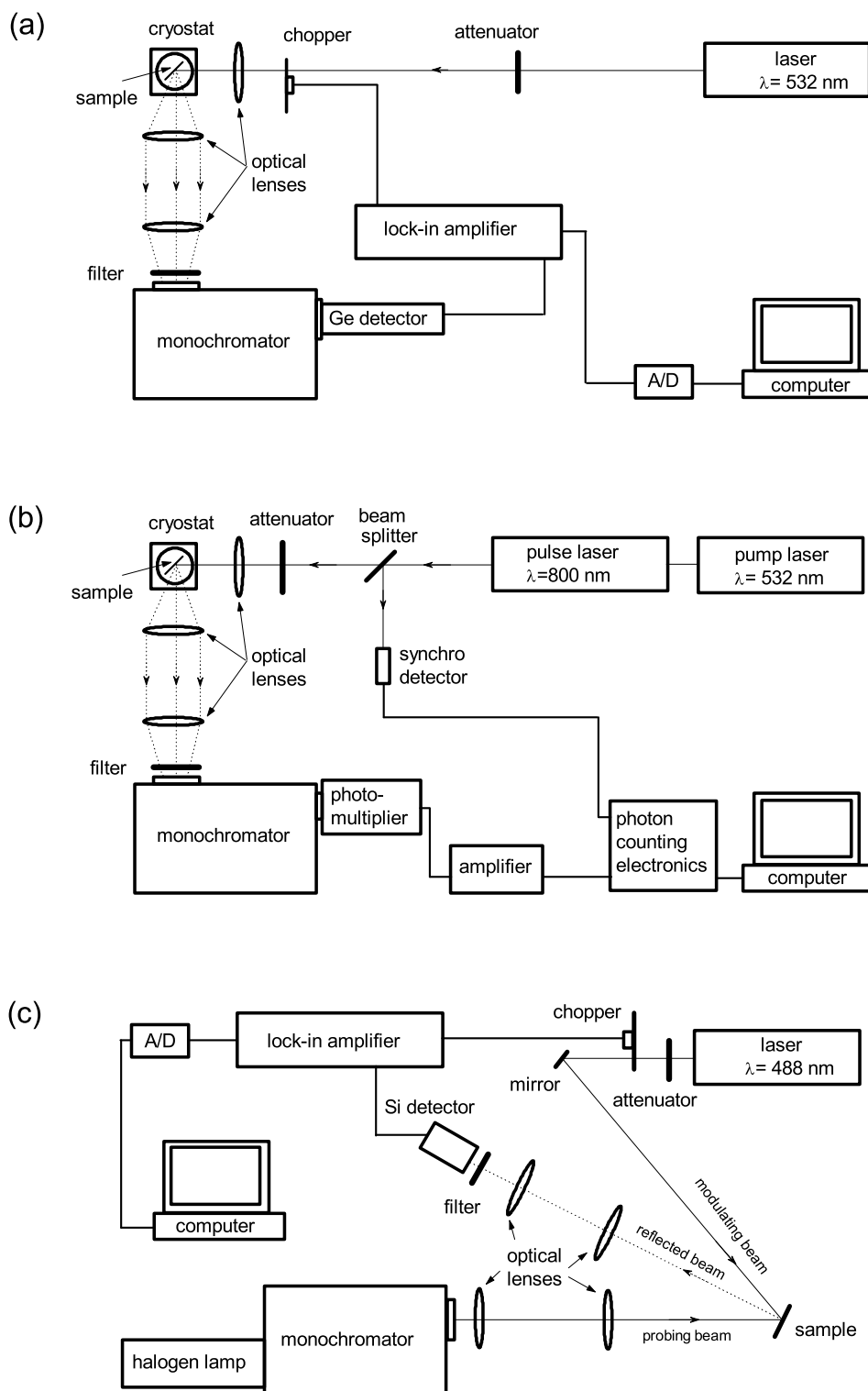


Figure 3.4: Schematic diagrams of (a) photoluminescence, (b) time-resolved photoluminescence, and (c) photoreflectance setups used in this work.

Schematic diagrams of the PL, TRPL, and PR setups used in this work are shown in Fig. 3.4(a), (b) and (c), respectively.

PL measurement is a widely-used, contactless, non-destructive spectroscopic characterization method of probing the energy states and different radiative recombination transitions in semiconductors [91]. When a laser beam with a sufficient photon energy is utilized for excitation, the incoming photons are absorbed by the sample and electron-hole pairs are created. The generated carriers quickly thermalize to near-band-edge states and then recombine either radiatively or non-radiatively. A typical PL spectrum is composed of several types of transitions. Common radiative transitions include the band-to-band transition, the transition from the conduction band to an acceptor state, and excitonic transitions. Therefore, the PL measurement is one of the most versatile tools for semiconductor characterization. Properties such as bandgap energy, impurity, and defect levels, recombination mechanisms, and checking material quality can be evaluated. All PL intensities mentioned in this thesis are the peak intensities of PL spectra.

TRPL is a special case of PL spectroscopy. In the TRPL measurement, the sample is excited with a laser pulse and the PL intensity at a chosen wavelength is monitored as a function of time delay after the excitation. A typical TRPL curve is an exponentially decaying PL transient. By fitting the measured curve with an exponential function, information about the electron relaxation and recombination mechanisms, including non-radiative channels, can be obtained. In this work, the TRPL transients of the passivated and unpassivated near-surface QWs were recorded at the wavelength of the maximum intensity of the continuous-wave PL peak. First order

$$y(t) = A_1 \exp(-t/\tau) + C, \quad (3.1)$$

or second order

$$y(t) = A_1 \exp(-t/\tau_1) + A_2 \exp(-t/\tau_2) + C \quad (3.2)$$

exponential function was fitted to the experimental data by adjusting the luminescence intensity A_i , carrier lifetime (PL decay constant) τ_i , and C ($i = 1, 2$). Parameter C takes into account the noise background present in the measurement. The carrier lifetime can be expressed as $\tau_i^{-1} = \tau_{R,i}^{-1} + \tau_{NR,i}^{-1}$, where $\tau_{R,i}$ and $\tau_{NR,i}$ are the radiative and non-radiative lifetimes, respectively. At low temperature, the passivated samples with less surface states showed a slow decay (larger carrier lifetime) whereas the unpassivated samples with higher density of surface states and non-radiative centers rapidly deplete the free-carrier population resulting in a much faster decay (smaller carrier lifetime).

PR is a contactless form of external modulation spectroscopy. The basic idea of the modulation spectroscopy is a very general principle in experimental physics. Instead

of measuring the optical reflectance (or transmittance) of a material, the derivative with respect to some parameter is evaluated [92]. In PR measurement, a light beam passes through a monochromator used for measuring the surface reflectance of the sample while the reflectance is periodically modulated by a laser beam with a higher photon energy than the energy bandgap of the sample. The modulation laser beam creates electron-hole pairs, which can recombine with the charge in surface states and, thereby, reduce the built-in electric field. These effects bring a lot of sharp spectral features into the modulated reflectance spectrum. The relative change in reflectance $\Delta R/R$ is recorded as a function of the energy (or wavelength) of the probing light. Based on the extrema positions of the Franz-Keldysh oscillations (FKOs) [93] in a PR spectrum, it is possible to calculate the surface electric field according to the relationship

$$m\pi = \phi + \frac{4}{3}[(E_m - E_g)/(\hbar\theta)]^{3/2}, \quad (3.3)$$

where m is the index of the m th extremum, ϕ is an arbitrary phase factor, E_m is the corresponding probe photon energy, E_g is the energy bandgap, and $\hbar\theta$ is the characteristic energy of FKOs [93, 94]. It is given by

$$(\hbar\theta)^3 = (q^2\hbar^2F^2)/(2\mu), \quad (3.4)$$

where F is the surface electric field, q is the magnitude of the electronic charge, and μ is the reduced effective mass of the material (for GaAs $\mu=0.056m_0$, [94]). Based on the equations above, the quantity of $(4/3\pi)(E_m - E_g)^{3/2}$ vs m should yield a straight line with a slope of $(\hbar\theta)^{3/2}$, and then the surface electric field can be calculated.

In this work, PL measurements were conducted by utilizing a diode-pumped frequency doubled Nd:YVO₄ laser emitting at 532 nm for excitation. Samples were placed in a closed-cycle helium cryostat and cooled to 10 K. A liquid-nitrogen-cooled germanium detector and standard lock-in techniques were used to record the PL spectra. The TRPL measurements were performed by exciting the samples with 150 fs pulses from a mode locked Ti:sapphire laser at 800 nm. The PL transients at selected wavelengths were detected by a Peltier-cooled microchannel plate photomultiplier and time-correlated single photon counting electronics. The approximate temporal resolution of the system was 30 ps. For the PR measurement, a 488 nm argon ion laser was used for modulation and a halogen lamp as the probing light source. The PR spectra were recorded with a Si p-n detector using standard lock-in techniques.

Since the optical properties of the samples are crucial factors for comparing the passivation effects, special attention was paid on the experimental setup and its alignment. In order to reduce the uncertainty caused by the system, all the optical lenses were carefully aligned and the luminescence collection was optimized for all the samples before each measurement. All the experimental parameters including

the laser excitation power were kept the same for each set of samples for comparing the passivation effects. However, variation between different growth runs and fluctuations across the same sample might bring some uncertainty for the measurement which can not be evaluated accurately.

4 GaAs surface passivation

This chapter discusses the results of publications I–IV. In these publications, techniques for the passivation of the GaAs surface by using different materials are studied.

4.1 In-situ epitaxial passivation of GaAs (100)

A straightforward and effective method to investigate surface states is to probe the optical properties of a near-surface quantum well (NSQW) [95]. When a QW is close to the surface, surface recombination leads to the reduction of the PL intensity and also to deterioration of the other characteristics of the QW. As a result, by comparing the optical properties of passivated and unpassivated NSQWs, one can find out whether the passivation has had any effect and one can compare the passivation efficiency of different materials.

Fig. 4.1 shows the schematic diagram of the NSQW structure used for investigating the surface passivation effect in publications I–IV. The NSQW structure consists of a 100-nm-thick GaAs buffer layer, a 4-nm-thick $\text{In}_{0.22}\text{Ga}_{0.78}\text{As}$ QW, and a 5-nm-thick GaAs capping layer grown on semi-insulating GaAs (100) (Publ. I, II, IV) or (110) (Publ. III) substrate. All the NSQW structures were grown at 650 °C and V/III ratios and growth rates used for GaAs and InGaAs layers were 27, 4.1 Å/s and 23, 4.9 Å/s respectively. Finally, ultra-thin passivation layer was grown by *in-situ* (publication I–III) or *ex-situ* (publication IV) methods on top of the NSQW structure. For reference, a similar sample without passivation and also a deep-QW sample with a 20-nm-thick capping layer were grown. A QW with a 20-nm-thick capping layer was used as a "deep" QW, because the PL intensity of the QW does not increase considerably even if the thickness of the capping layer is increased further [55].

In publication I, the passivation effects of epitaxially grown thin GaN and InP layers were compared. A 1-ML-thick InP or GaN layer was grown on the GaAs top barrier as the passivation layer. The InP passivation layer was grown at 650 °C while the GaN passivation layer was grown at 550 °C based on the previous study of growth of cubic GaN on GaAs [96, 97]. Another type of passivation was performed using As–N

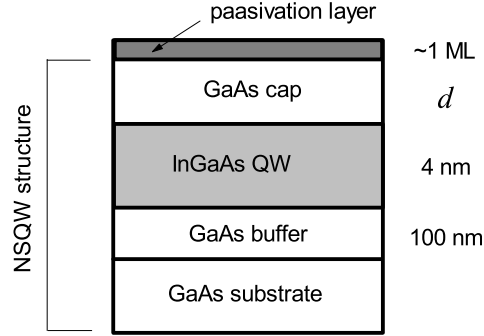


Figure 4.1: Schematic diagram of the NSQW structure used in this work for studying the surface passivation effect. The thickness of the GaAs capping layer d is changed in different samples. In the NSQWs for *in-situ* passivation $d= 5$ nm; in the NSQWs for *ex-situ* passivation $d= 5$ nm or $d= 3$ nm; and in the reference deep-QWs $d= 20$ nm.

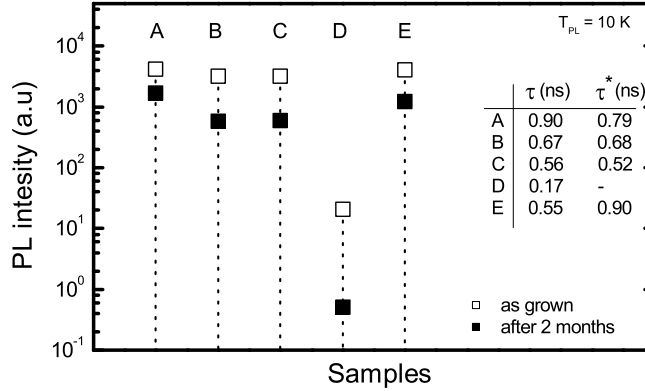


Figure 4.2: Comparison of the low-temperature PL intensity of passivated and unpassivated samples immediately after growth (as-grown) and after two months exposed to air. The inset shows a table of carrier lifetimes for the as-grown (τ) and air exposed (τ^*) samples. The samples are InP-passivated (A), GaN-passivated (B), nitridated (C), unpassivated (D), and deep-QW (E). [Publ. I]

exchange to nitridate the GaAs surface by exposing the sample to dimethylhydrazine (DMHy) during the sample cooling from 650 °C to 400 °C. All these passivation methods were observed to significantly enhance the PL intensity and the carrier lifetime and to reduce the surface electric fields.

Fig. 4.2 shows the low-temperature PL intensities of the unpassivated and passivated NSQWs before and after two months air exposure. The carrier lifetime, determined by exponential fits $exp(-t/\tau)$ to the TRPL transients, of as-grown (τ) and air exposed (τ^*) samples are also shown in same figure as an inset. It can be clearly seen that the PL intensities of all the passivated NSQW samples experience a strong

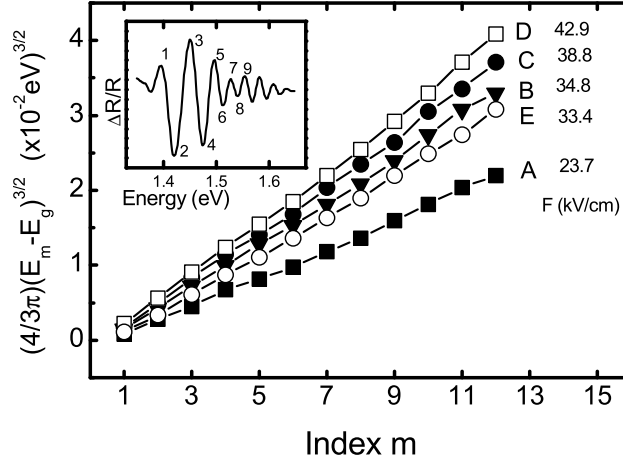


Figure 4.3: The calculated value of $(4/3\pi)(E_m - E_g)^{3/2}$ as a function of the extremum peak index m of PR spectrum for as-grown samples. The inset shows a PR spectrum with the extremum peak indices m marked to the spectrum. The calculated values of the surface electric field of each sample are also shown. The samples are InP passivated (A), GaN passivated (B), nitridated (C), unpassivated (D), and deep-QW (E). [Publ. I]

enhancement compared to that of the unpassivated one. The enhancement factor for the as-grown samples is about 200 and the InP passivation shows the best passivation efficiency. The GaN passivated and surface nitridated samples show almost comparable PL intensities to the deep QW. After storing the samples two months in the air ambient, the PL intensities of all the samples were reduced but the unpassivated sample degraded severely. The PL intensities of the passivated samples are more than three orders of magnitude larger. The results of the carrier lifetimes agree with the PL intensity result: in passivated samples the carrier lifetime is increased notably compared to that of the unpassivated sample. However, after two months in air ambient, the carrier lifetime of the unpassivated NSQW can not be determined due to the too low luminescence intensity. Moreover, the deep-QW shows a longer carrier lifetime after air exposure, which is assumed to be caused by the inhomogeneity of the growth across the sample.

The passivation effect to the surface electric field was studied with the room temperature PR measurement. Fig. 4.3 shows the value of $(4/3\pi)(E_m - E_g)^{3/2}$ as a function of the extremum peak index m . The inset shows the extremum peak indices of a PR spectrum. The calculated surface electric fields of the InP passivated, the GaN passivated and the unpassivated samples are 23.7, 34.8 and 42.9 kV/cm, respectively. This result is comparable with the earlier reports on the surface fields of phosphor and sulphur passivated samples [39]. From these values, it can be clearly seen that the InP and GaN surface passivation layers can efficiently reduce the surface electric field. Comparing the NSQW and the deep QW samples, the calculated value of sur-

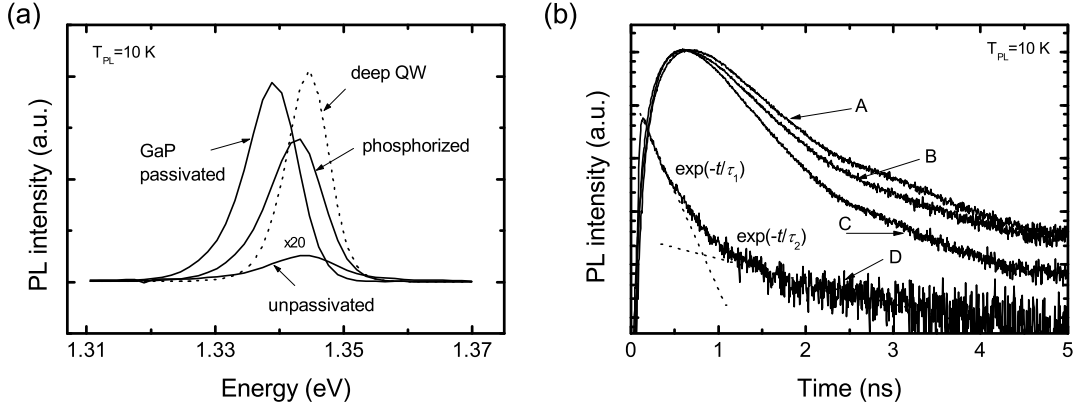


Figure 4.4: (a) Low-temperature PL spectra and (b) low-temperature TRPL transients of surface phosphorized (A), GaP-passivated (B), deep QW (C) and unpassivated near-surface QW (D) samples. [Publ. II]

face electric field is larger in the NSQW. When the QW is near to the surface, there is an accumulation of carriers into the QW. This new carrier distribution causes a different electric field.

Surface phosphorization was considered to be an effective way of GaAs surface passivation via on the surface forming a thin GaP layer which has smaller oxidation rate compared to GaAs. The earlier studies reported a two orders of magnitude enhancement in the PL intensity and a reduction of surface electric fields in the phosphor treated samples [38, 39]. In publication II, the GaAs surface passivation by both As–P exchange and an epitaxially grown ultra-thin GaP layer is studied. First, growth conditions for a thin GaP layer on the GaAs surface were optimized. By changing the growth condition of the GaP passivation layer, it was found out that a 1-ML-thick GaP layer covering the surface two dimensionally can be grown with the V/III ratio of 130 on an InGaAs/GaAs NSQW structure. The best passivation effect was achieved at the growth temperature of 580 °C in the range of 550–600 °C. Varying the thickness of the GaP passivation layer from 1 ML to 3 ML and changing the V/III ratio to higher values did not bring any significant changes in the surface morphology or the PL intensities of the NSQW structures. The surface phosphorization was realized by exposing the samples to a TBP flow of 330 $\mu\text{mol}/\text{min}$ during the cooling from 600 °C to 400 °C after the growth of the GaAs cap layer.

Fig 4.4 shows the low-temperature PL spectra and TRPL transients of the GaP passivated, the surface phosphorized and the unpassivated reference samples. In both passivation methods, the PL intensities of the passivated NSQWs are increased by a factor of more than 150. TRPL transients of all the samples exhibit a double exponential decay (Fig 4.4(b)). This may be related to the band-bending caused by surface states [98] or exciton transfer between the continuum (free carriers) and the bound states [99]. The PL decay times (carrier lifetimes) were determined by using the second order exponential fit. The decay time τ_1 was increased in both the

passivated samples (>0.5 ns) compared to the unpassivated sample (0.36 ns) while τ_2 remained almost unchanged (2.2–2.5 ns). The increase of τ_1 in the passivated samples can be attributed to the decrease of non-radiative recombination in the early stage of the decay [100, 101] due to reduced surface state density. On the other hand, at the later stage of decay the main contribution to the luminescence intensity probably comes from the electron hole recombination of another carrier population which is less affected by the surface states so that the decay constants for all the samples are almost the same.

4.2 Growth on and surface passivation of GaAs (110)

GaAs (100) is the most widely used GaAs orientation in research and in applications. For higher crystal indices, however, GaAs (110) is one of the most widely studied orientations [102, 103]. Therefore, the passivation of GaAs (110) is essential in some cases. For example, QW lasers grown on GaAs (100) substrates have (110)-oriented mirrors. Destruction of laser mirror surfaces due to the overheating caused by optical absorption on the surface states is the most significant factor limiting the power density of high-power lasers [104, 105]. Better passivation methods for (110) surfaces might improve the laser performance.

Epitaxial growth of bulk [106] and QW [107] structures on GaAs (110) substrate has been studied in MBE systems in detail. In these research works the surface morphologies of the epitaxially grown layers were found to be faceted with triangular shaped islands with densities of approximately 10^6 cm⁻² [106]. The explanation for the formation of such islands on GaAs (110) surface has been discussed in detail [106, 108, 109]. The bonding of the Ga and As atoms naturally exposes both types of (111) planes on the (110)-oriented GaAs surface, as shown in Fig 4.5. Kinetic studies have shown that the incoming As atoms are strongly attracted to the stable (111) Ga surface and will bond there faster than Ga atoms bond to the (111) As surface. These chemisorbed atoms will then provide a basis for further chemisorption of the incoming Ga and As atoms. As a result, a facet begins to form from the fast growing (111) Ga surface with sides of (100) and (010) filling in and, thus, creating the facet shape and, consequently, resulting in a triangular shaped island.

In publication III, the QW growth on and surface passivation of GaAs (110) substrates were studied. In addition to the (110) samples, the same structure was also grown on a (100) substrate in the same growth run. In order to study the surface morphology and structural properties of the epitaxially grown layers on the GaAs (110) substrate, a single GaAs layer and an In_xGa_{1-x}As multi- QW (MQW) structure were grown with different growth parameters and layer properties. Triangular shaped small islands were observed on both the GaAs and the MQW surfaces. Fig. 4.6 shows AFM images of as-grown GaAs layers with the thickness of 10 nm and 100 nm. The average base size and the average height of a typical island are 100 nm

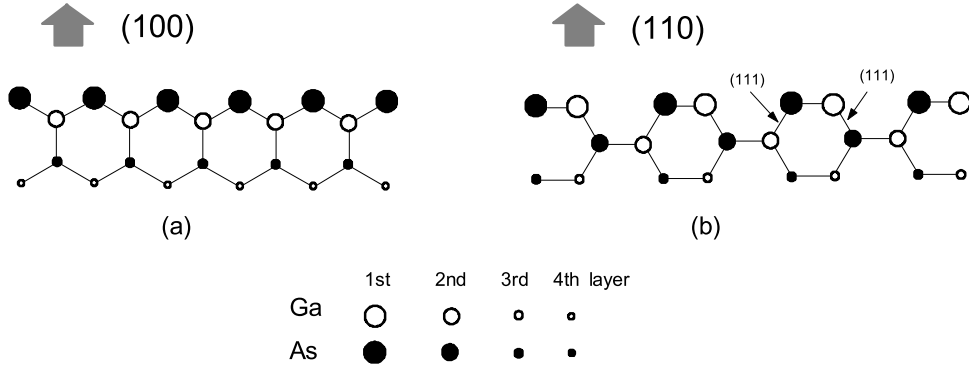


Figure 4.5: Atomic structure of ideal (a) GaAs (100) and (b) GaAs (110) surfaces. [110].

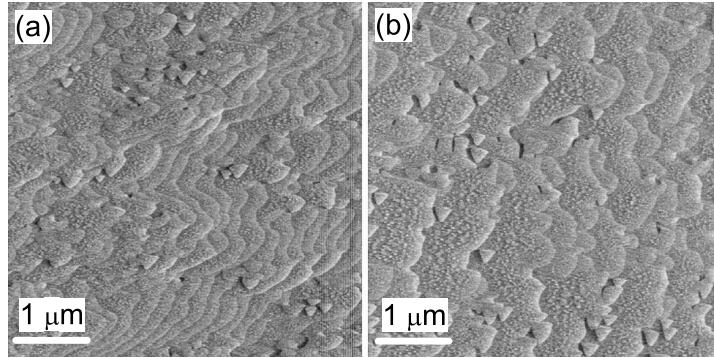


Figure 4.6: AFM images from the surface of GaAs layers (grown at 650 °C) on GaAs (110) substrate with the thickness of (a) $d = 10$ nm and (b) $d = 100$ nm. The scan size is $5 \times 5 \mu\text{m}^2$ and the vertical scale is 5 nm. [Publ. III]

and 1-2 nm, respectively. The approximate density of the islands is 10^7 cm^{-2} when the GaAs layer thickness is 10 nm. Changing the thickness of the GaAs layer from 10 to 100 nm results in a slight decrease in the island density. Similar morphologies were also observed on the MQW surfaces. Variation of the growth temperature and the V/III ratio of MQWs did not have significant effect on the shape and size of the islands, but the density of the islands decreased slightly compared to that on the single GaAs layer. Based on these results, it is assumed that the island characteristics of the epilayers are caused by the original facet-structured surface of the GaAs (110) substrate.

The MQW samples were also studied by X-ray diffraction measurement to estimate the thicknesses of the InGaAs QWs and the GaAs barriers. Almost the same parameter values were obtained for the same MQW structure on GaAs (100) and (110) substrates in a wide range of growth temperatures. Similar optical properties, i.e., PL peak positions and intensities, were also obtained. Apart from the island-related

Table 4.1: Key characteristics of the PL and TRPL measurement results for various passivated near-surface QWs on GaAs (110) and GaAs (100) substrates. The PL intensity of the unpassivated near-surface QWs have been normalized to 1.

Substrate	Sample	PL intensity	FWHM (meV)	τ_1 (ns)	τ_2 (ns)
110	unpassivated	1	24.9	0.46	2.1
	deep QW	132	14.2	0.69	2.3
	GaP-passivated	96	18.5	0.81	2.2
	phosphorized	115	17.2	0.86	2.4
	InP-passivated	72	19.4	0.77	2.2
100	unpassivated	1	16.2	0.33	2.7
	deep QW	162	10.3	0.51	2.8
	GaP-passivated	101	10.6	0.56	2.7
	phosphorized	123	10.7	0.69	2.9
	InP-passivated	135	13.6	0.63	2.8

characteristics of the (110) surfaces, the structural quality and the optical quality of the InGaAs MQWs grown on GaAs (110) substrates were similar to those grown on GaAs (100) substrates. This indicates that similar high quality QWs can be obtained by MOVPE fabrication using the same growth conditions on both (110) and (100) GaAs substrates.

The passivation of the (110) GaAs surface was studied by investigating the optical properties of a single NSQW while a nominally 1 ML thick GaP and InP layers as well as surface phosphorization were applied as passivation methods. The small islands can still be seen on both the unpassivated and passivated (110) QW sample surfaces. On the other hand, the clear atomic layer terraces were observed on the unpassivated and passivated (100) QW sample surfaces. The results of the PL and TRPL measurements are summarized in Table. 4.1.

From Table 4.1, it can be seen that the PL intensity of the passivated samples is significantly increased on both substrates and the enhancement factor is up to two orders of magnitude. The PL decay time τ_1 is almost doubled in all the passivated samples while τ_2 remains almost unchanged. The different effect of passivation on the two lifetimes can be understood if one assumes that the rapidly decaying carrier population is interacting with the surface states and the slowly decaying population is not. The large values of τ_2 hint that the luminescence could come from a spatially separated populations of electrons and holes. The enhancement of the PL intensity via passivation is much larger than the enhancement of carrier lifetimes could be expected from the change of τ_1 . The additional enhancement could be caused by the electric field near the surface enabling more carriers to reach the NSQW.

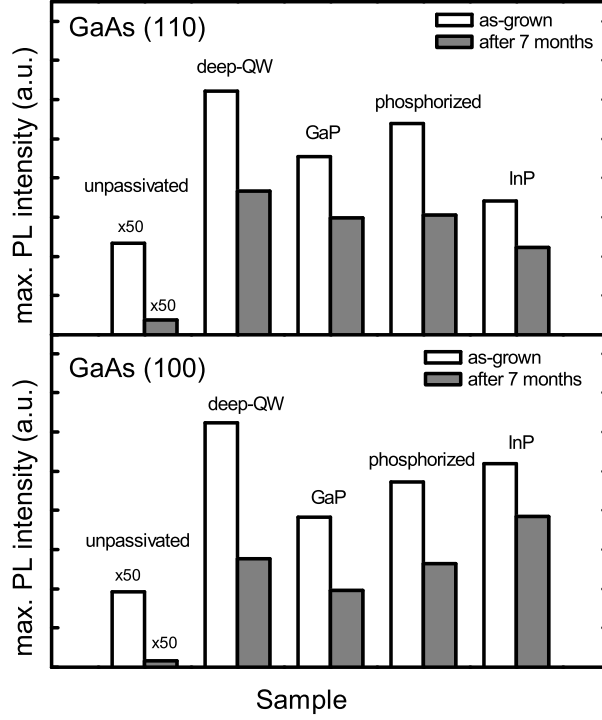


Figure 4.7: Comparison of the low-temperature PL intensity of as-grown and samples exposed to air ambient for seven months passivated and unpassivated QWs on both GaAs (110) and (100) substrates. For clarity, the PL intensity of unpassivated samples is multiplied by a factor of 50. [Publ. III]

However, different passivation methods show different passivation efficiencies depending on the substrate orientation. The largest PL enhancement on the (110)-oriented NSQW is obtained by surface phosphorization with TBP while the ultra-thin InP layer passivation is the best on the (100)-oriented NSQW. The PL decay time τ_1 is increased notably in all the passivated samples. However, the values of τ_1 in (110) QWs are a little higher than those of the (100) QWs, i.e., $(\tau_1)_{110} > (\tau_1)_{100}$. It seems that at the later stage of decay, a carrier population separated from the surface states dominates the behavior, because the values of τ_2 in both the passivated and unpassivated samples are approximately the same. But the value of τ_2 in (110) near-surface QWs seems to be somewhat lower than that in (100) QWs, $(\tau_2)_{110} < (\tau_2)_{100}$. The PL intensities of all the samples were measured with the same setup after keeping them in the air ambient for seven months, in order to investigate the time durability of the passivation effect. Comparison of the PL intensity of the passivated and unpassivated (110) and (100) QWs are shown in Fig. 4.7. The PL intensities of all the samples are reduced over time by approximately 20–40%. However, the degradation of the PL intensity of the unpassivated QW is faster on the (100) substrate.

All these results indicate that the QWs grown on (110) and (100) substrates behave

Table 4.2: The overall differences of optical properties of QW structure on GaAs (110) and (100) substrates. γ is the ratio of the initial PL intensity of the QW to that after 7 months of air exposure, i.e., $\gamma=I_0/I_{7months}$.

PL peak	$(\text{FWHM})_{110} > (\text{FWHM})_{100}$
PL intensity degradation	$(\gamma)_{110} < (\gamma)_{100}$
TRPL transient	$(\tau_1)_{110} > (\tau_1)_{100}$ $(\tau_2)_{110} < (\tau_2)_{100}$

differently. These overall differences are listed in Table 4.2. The differences are probably caused by the different physical properties of the GaAs surfaces. On GaAs (100) substrate, the more severe degradation of the PL intensity and the smaller PL decay time at the early stage of the decay (τ_1) indicate that the density of surface states and non-radiative recombination centers is generally higher compared to those of (110)-oriented GaAs. The smaller values of τ_2 in GaAs (110) maybe related to the larger surface energy band bending due to the surface lattice relaxation [111, 112] on the (110)-oriented epilayer. As for the broader PL emission (larger FWHM) from the (110) QWs, it may be caused by the fluctuation of indium composition of the InGaAs layer due to the island formation.

4.3 Ex-situ passivation with titanium nitride

In publication IV, the suitability of *ex-situ* GaAs surface passivation by using an ALD grown TiN layer was investigated. The TiN layer was deposited at 275 °C using titanium tetrachloride (TiCl₄) and ammonia (NH₃) as precursors. Two sets of MOVPE grown NSQW samples; series A with a 5-nm-thick GaAs capping layer and series B with a 3-nm-thick GaAs capping layer, were used to study the passivation effects. The thicknesses of TiN layers were determined by the measured and simulated x-ray reflectivity (XRR) curves of TiN layers grown on GaAs substrates with 20, 60, and 100 growth cycles (2.0, 3.9, and 5.6 nm, respectively).

Fig. 4.8(a) shows the PL intensity of the TiN-passivated samples from series A and series B as a function of the passivation layer thickness. In both series, the PL intensities increased significantly and the enhancement factor is up to 15 times compared to the unpassivated (zero cycles) reference sample. The maximum PL intensity is obtained when the TiN layer is about 4 nm thick (60 cycles). The samples in series B show deteriorated PL intensities after one month of exposure to air, especially for the thin layers (0–3 nm).

Fig. 4.8(b) shows the low-temperature TRPL transients and the fitted carrier lifetimes for an unpassivated reference, a TiN passivated NSQW, and a deep QW from

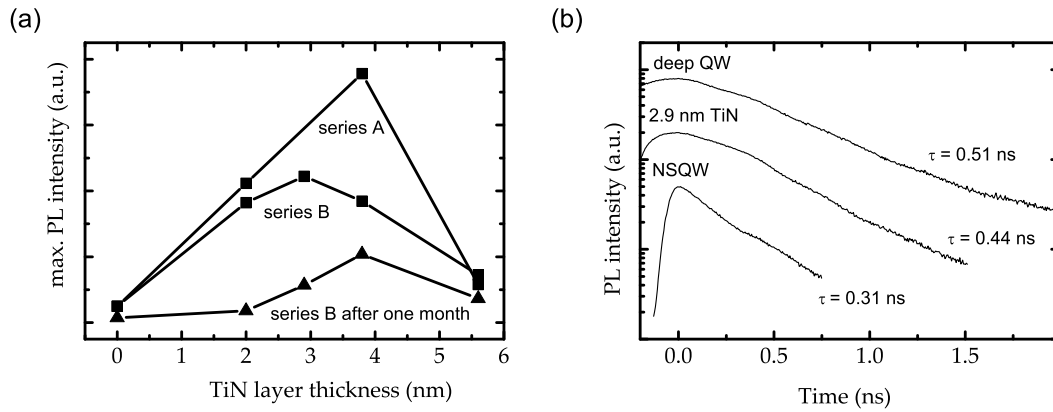


Figure 4.8: (a) Low-temperature PL intensities of TiN passivated (series A and B) NSQWs as a function of TiN layer thickness. (b) Low-temperature TRPL transients of an unpassivated NSQW, a TiN passivated NSQW, and a deep QW samples from B series after one month air exposure. [Publ. IV]

series B. All the samples were exposed for one month in the air ambient. The decay times τ were determined from the transients by using first-order exponential fits. The result agree with the PL measurement since the carrier lifetime is increased in the passivated samples. These results show that the passivation of the GaAs surface can be performed by an *ex-situ* epitaxial method, i.e., the ALD process, and the passivation efficiency is considerable.

5 Self-assembled InAs/GaAs quantum ring structures

This chapter discusses the results of publications V and VI. In publication V, self-assembled formation of InAs islands on GaAs (110) substrates was studied. Transformation of InAs islands into rings by using a thin partial capping layer on GaAs (100) substrate was studied in publication VI.

5.1 Self-assembled InAs island formation on GaAs (110)

A lot of research has been devoted in the last two decades to realizing the predicted potential of zero-dimensional (0D) quantum confined structures, i.e., quantum dot (QD) structures. QDs are expected to have many interesting and useful properties for optoelectronic device applications. One of the applications in which these properties can be utilized is the QD laser [113]. The most straightforward technique to produce QDs is to fabricate quantum wells by MOVPE or MBE and then etch mesas with lateral dimensions in the range of 10–100 nm. However, the non-radiative defects produced during the etching procedure lead to the degradation of the material quality. The development of self-assembled growth of nanoscale islands makes it possible to avoid these defects. Particularly, the coherent S-K growth mode has been utilized successfully in the In(Ga)As/GaAs material system [114].

InAs island formation on GaAs (100) has been widely studied and the growth mechanism is well understood. The transition from 2D to 3D nucleation occurs prior to the incorporation of dislocations. However, reflection high-energy electron diffraction (RHEED) studies have shown that the formation of 3D nuclei is completely suppressed during growth on (110) surfaces [115]. The InAs epilayer remains 2D irrespective of the thickness and the strain relaxation occurs by formation of misfit dislocations instead of 3D islands. If the occurrence of the 3D growth mode was only dependent on strain, it should be independent of the substrate orientation since the lattice mismatch (about 7.1%) is always the same for InAs islands on GaAs regardless of orientation. So, this observed growth behavior of InAs on GaAs (110) must be related to the unique properties of this surface orientation.

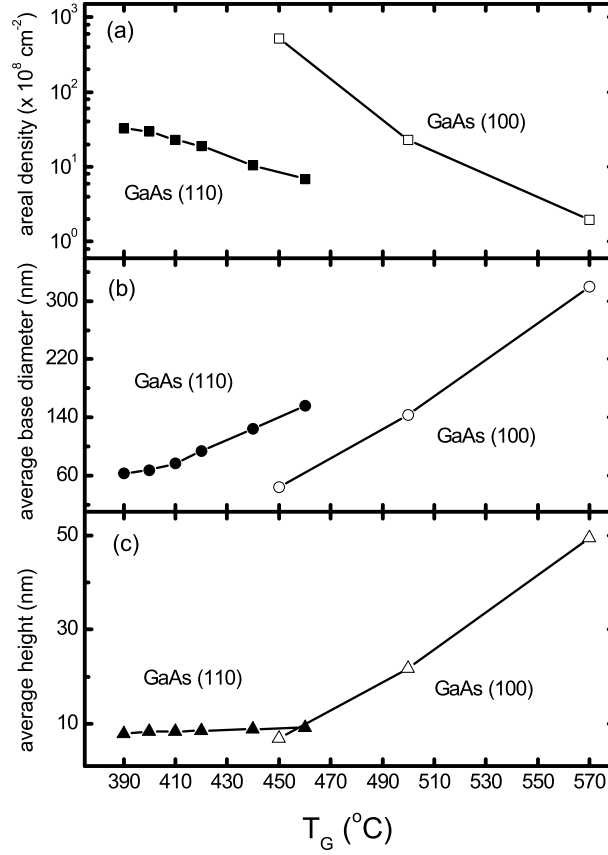


Figure 5.1: (a) Areal density, (b) average base diameter, and (c) average height of InAs islands on GaAs (110) and GaAs (100) as functions of the growth temperature. The nominal thickness of InAs layer is 1.7 ML, the growth rate is 1.5 ML/s, and the V/III ratio is 5. [Publ. V]

However, it has been recently reported that the substrate orientation is not an insurmountable obstacle for 3D island formation. A thin strain reducing (SR) layer has been observed to play a very crucial role in the formation of InAs islands on GaAs (110). For instance, InAs 3D islands have been successfully grown on GaAs (110) by using a few monolayers (MLs) of AlAs [116] and InGaAs [117] as a SR layer instead of growing islands directly on GaAs. Although the island growth on GaAs (110) typically results in a smaller island density than on GaAs (100), it shows potential for the position control of the QDs [118, 119] and for creating QD arrays by cleaved-edge overgrowth [116, 117].

In publication V, InAs island formation on GaAs (110) substrate was investigated by using a 3-ML-thick $\text{In}_{0.2}\text{Ga}_{0.8}\text{As}$ layer as a SR layer. The InAs layer was grown at different growth temperatures, layer thicknesses, growth rates and V/III ratios. For comparison, the same structure was also grown on a GaAs (100) substrate in a separate growth run due to the different growth temperature needed for island formation. For the study of optical properties, some samples were fabricated by

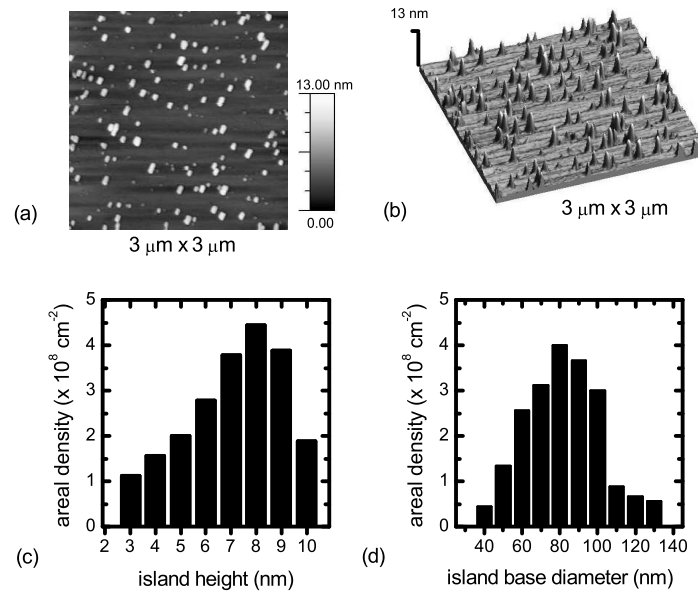


Figure 5.2: (a) 2D and (b) 3D images of the AFM scan from a sample with nominally 1.5 ML of InAs grown on GaAs (110) at 400 °C with a V/III ratio of 5. (c) Height and (d) base diameter distribution histograms of the islands. [Publ. V]

covering the islands with a 50 nm thick GaAs layer grown at the same temperature.

When 2 MLs of InAs was deposited on GaAs (110) and (100) substrates at 460 °C with and without the SR layer, 3D InAs islands were formed on GaAs (100) in both cases. By contrast, islands were observed on GaAs (110) only when the SR layer was used. The probable main role of the InGaAs SR layer on GaAs (110) substrate is in controlling strain and dislocation formation by forming In(Ga)As alloy rather than pure InAs in the beginning of the island deposition [117]. Thus, the preferred route for strain relaxation is formation of 3D islands.

Fig. 5.1 shows some basic properties, i.e., the areal density, the average base diameter and the height of the InAs islands grown on GaAs (110) and (100) substrates as a function of the growth temperature. On both substrates, as expected, the island density decreases and the island size increases when the growth temperature is increased. Fig. 5.2 shows AFM images as well as the island height and base diameter distribution histograms of typical InAs islands (1.5 ML InAs deposited at 400 °C) on GaAs (110). The aspect ratio (height/base diameter) is on average around 0.1. The aspect ratio of a typical island on (100) GaAs, grown at 460 °C, is about 0.15. These values coincide with the reported values of InAs/GaAs island aspect ratios of 0.1-0.25 [120].

However, some clear differences between the substrate orientations can be observed.

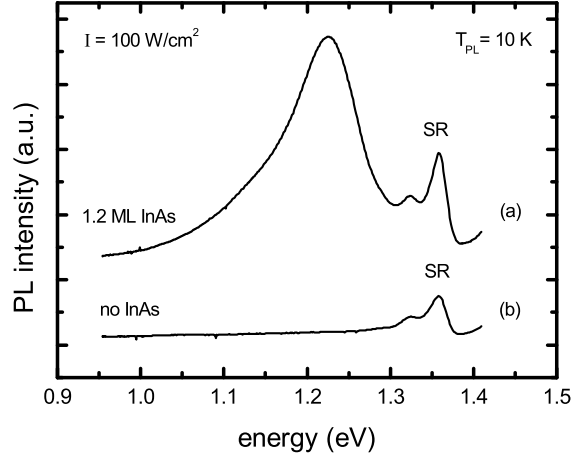


Figure 5.3: Low-temperature (10 K) PL spectra from (a) a sample containing capped islands grown on GaAs (110) (1.2 ML InAs grown at 460 °C) and (b) a reference sample without islands. The excitation intensity is 100 W/cm². [Publ. V]

For the (110) substrate, the island density is about 10^8 - 10^9 cm⁻² when the growth temperature is varied in the range of 390-460 °C. Above 460 °C, the islands become very large and below 390 °C no islands are formed. For the (100) substrate, on the other hand, the island density is two orders of magnitude larger at 460 °C. At growth temperatures lower than 450 °C, the (100) sample surface became very rough due to coalescence of the high density islands. The size, i.e., the base diameter and the average height, of the islands on the (100) substrate increased rapidly with the growth temperature. However, comparing these results to those carried out in MBE, the island size in this work is much bigger. There is no any direct proof that indicate whether the islands are coherent or not, or strongly alloyed with the substrate. This point will be clarified in our future research with the help of other characterization methods, e.g., transmission electron spectroscopy. On the other hand, only the lateral size of the islands on the (110) substrate increased when the growth temperature was increased. This behavior may be caused by a ripening process [121]. During ripening, when the island size reaches a certain crucial size, dislocation formation relaxes the strain energy of the islands, allowing the fast growth of dislocated islands in the lateral directions compared to that in the growth direction. A similar restriction of the island height due to the ripening effect was also reported on InAs islands grown on GaAs (100) substrates when the thickness of the InAs layer is continuously increased [122, 123]. Another possible reason for this behavior is that the critical thickness of dislocation-free islands is related to the energy barrier of dislocation formation [124] and/or an elastic strain effect [125] which are reported to depend on the substrate orientation [126]. If we assume that the critical thickness of the dislocation-free islands on the (110)-oriented substrate is smaller than that on (100) orientation, then the additional material is not deposited on the existing

islands, but is consumed in the nucleation of new islands. So, when same amount of material deposited on these two kinds of substrates more islands will be formed instead of increasing island height on the (110) substrate.

Properties of InAs islands on GaAs (110) were also studied by changing the other growth parameters, such as the nominal thickness of the InAs layer, the V/III ratio and the growth rate at growth temperature of 400 °C. No 3D islands were observed when the nominal thickness of InAs was less than 1.5 ML. When the thickness is increased further, the island density increases, but, unlike on the (100) substrate, the islands become smaller in both base the diameter and the height. The probable reason for this is that more InAs is deposited between the already-existing islands rather than on top of them due to the energy barrier of adatom incorporation [125]. As a result, the larger islands (with higher strain) tend to grow slower than the smaller islands. This also leads to formation of new islands.

Fig. 5.3 shows the low-temperature PL spectra of buried samples with and without InAs islands on GaAs (110). The PL peak from the InGaAs SR layer is seen in both of the spectra around 1.35 eV. However, a double PL peak is observed from the SR layer in both cases in Fig. 5.3. It is probably caused by monolayer variation of the thickness of the SR layer. The PL peak from the InAs islands is observed at 1.22 eV and has a full width at half maximum of about 100 meV. The broadness of the PL peak may be due to the inhomogeneity of the island size or the formation of intermixed $\text{In}_x\text{Ga}_{1-x}\text{As}$ islands with a wide range in the composition parameter x .

5.2 Transformation of InAs islands into quantum rings

Transformation of InAs islands into QRs on GaAs (100) substrate by using a GaAs partial capping layer was investigated in publication VI. InAs islands were formed by depositing a nominally 1.7-ML-thick InAs layer on a 100 nm GaAs buffer layer with a growth rate of 1.5 ML/s and a V/III ratio of 10. Before the InAs deposition, the reactor temperature was stabilized at the InAs growth temperature T_g (500–600 °C) under protective TBAs flow. InAs islands were transformed into QRs by capping the islands with a 2-nm-thick GaAs partial capping layer followed by annealing under TBAs flow. The growth rate of both GaAs partial capping layer and GaAs buffer layer was 4.1 Å/s. The annealing time, t_a , was 60 s and the annealing temperature, T_a , was the same as the island growth temperature, $T_a = T_g$. The annealing parameters T_a , t_a and the thickness of the partial capping layer, d_c , were varied to study their effects on surface morphology. Reference InAs island samples were taken out from the reactor right after the island growth and cooling down under TBAs flow. Samples for the PL measurement were covered with a 50-nm-thick GaAs barrier layer at the annealing temperature T_a after the QR transformation was completed.

Fig. 5.4 shows 2D and 3D AFM images of QRs grown at different temperatures.

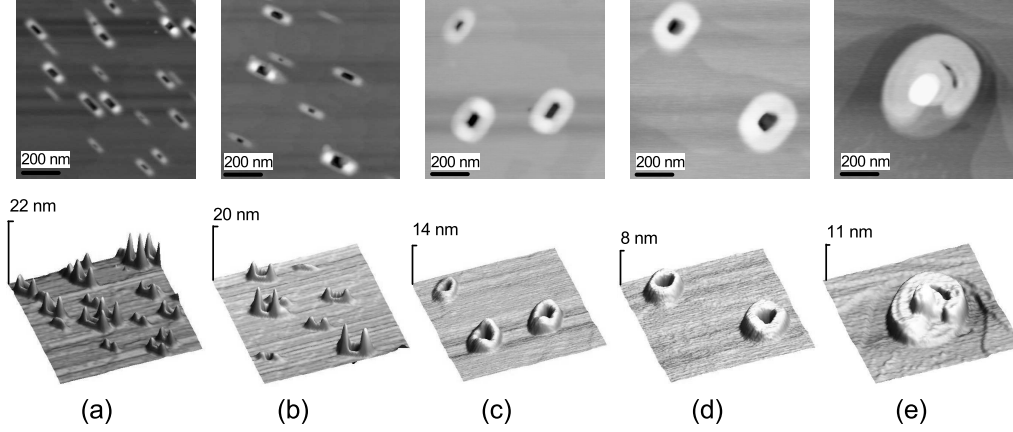


Figure 5.4: 2D and 3D AFM images of InAs QRs fabricated at different temperatures: (a) 500 °C, (b) 530 °C, (c) 550 °C, (d) 570 °C, and (e) 600 °C. The thickness of the capping layer is $d_c = 2$ nm and the annealing time is $t_a = 60$ s in all the samples. The size of all the images is $1 \mu\text{m} \times 1 \mu\text{m}$. Samples were grown on GaAs (100) substrate. [Publ. VI]

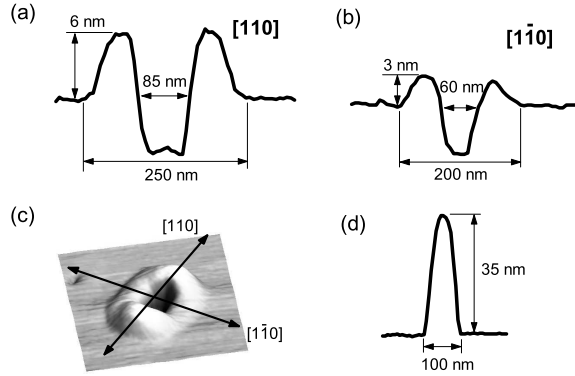


Figure 5.5: (a) $[110]$ and (b) $[1\bar{1}0]$ cross-sectional profile of a typical QR grown at 550 °C by covering InAs islands (nominal thickness of 1.7 ML) with a 2 nm GaAs partial capping layer. (c) A 3D AFM image of the QR with the crystal directions indicated. (d) The cross-sectional profile of an InAs island grown at 550 °C. [Publ. VI]

Island-to-ring transformation results in significant changes in the morphology of the QRs compared to those of the initial islands. First, the areal density of the QRs become smaller than that of the original islands. The difference is larger when the growth temperature is higher. At 570 °C, the QR density ($\sim 10^8 \text{ cm}^{-2}$) is about one quarter of the initial island density. In the reference samples, no obvious differences were observed between the areal density of InAs islands with and without the 15 s stabilization (pause between growth of the islands and the partial capping layer). Therefore, it was assumed that the reduction of the QR density is related to the temperature dependence of the indium atom diffusion during the annealing

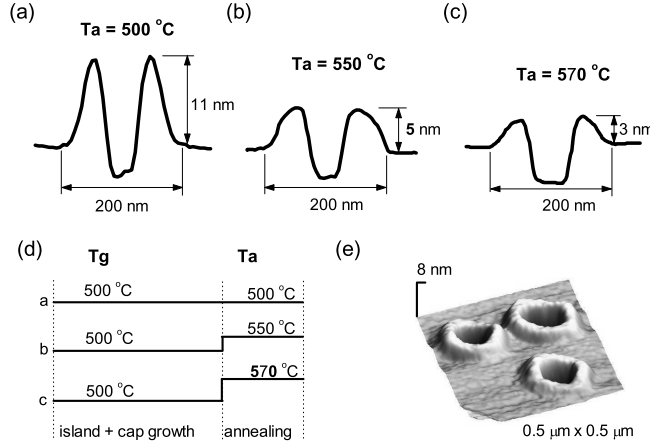


Figure 5.6: Comparison of [110] cross-sectional profiles of QRs, grown at $T_g = 500\text{ }^\circ\text{C}$, and annealed at different temperatures: (a) $T_a = 500\text{ }^\circ\text{C}$, (b) $T_a = 550\text{ }^\circ\text{C}$, and (c) $T_a = 570\text{ }^\circ\text{C}$ ($d_c = 2\text{ nm}$, and $t_a = 60\text{ s}$). (d) Temperature sequence during fabrication of the QR samples shown in (a), (b) and (c). (e) 3D AFM image of the QRs grown at $T_g = 500\text{ }^\circ\text{C}$ and annealed at $T_a = 570\text{ }^\circ\text{C}$. [Publ. VI]

of the partially capped islands. At higher annealing temperature, the mobility of the indium atoms is much higher and equivalent in all directions. Under these conditions, small islands can become larger in lateral dimensions or even overlapped with the neighboring islands. Also, it is possible that the material from the smaller islands diffuses to the bigger islands. Secondly, the lateral distance of the QR is increased and the height is decreased. The lateral distance of the outer and the inner edge of the rim and the rim height are different for [110] and $[1\bar{1}0]$ directions (Fig. 5.5). However, the camel-hump shape of the QRs is more obvious at lower growth temperatures (Figs. 5.4(a) and (b)) while the QRs are closer to the perfect ring shape at higher growth temperatures (Fig. 5.4(c) and (d)). The elongation of QRs in [110] direction may be explained by the different diffusion constant of the indium atoms, much faster along $[1\bar{1}0]$ than along [110] direction [83], which can be attributed to the chemical reactive anisotropy of the group III migrating atoms [74]. Compared to the average size of a typical island grown at the same temperature, the lateral distance of the QR is increased by over two times and the height is decreased by about 6-10 times.

To investigate the effect of growth conditions on ring formation, QR structures were fabricated by varying t_a and d_c while keeping the other parameters the same. When the annealing time t_a is short, most of the islands did not completely transform into rings. Same suppression of QR formation was also observed when the thickness of the partial capping layer was over 5 nm. The optimum values for t_a and d_c were found to be 60–120 s and 0.5–2.0 nm, respectively.

Besides the annealing time, the annealing temperature also affects QR formation sig-

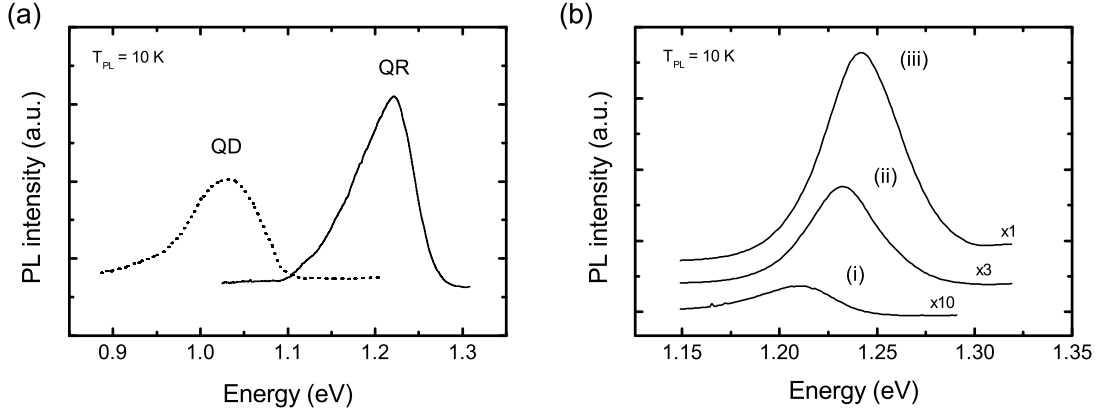


Figure 5.7: (a) Low temperature (10K) PL spectra of buried InAs islands (QDs) and QRs. InAs islands with nominal thickness of 1.7 ML were grown at $T_g = 550$ °C, QRs were transformed from these islands by using $d_c = 2$ nm, $t_a = 60$ s and $T_a = T_g = 550$ °C. (b) Low temperature (10K) PL spectra of buried QRs grown at $T_g = 500$ °C, and annealed at different temperatures: (i) $T_a = 500$ °C, (ii) $T_a = 550$ °C, and (iii) $T_a = 570$ °C ($d_c = 2$ nm, $t_a = 60$ s). The excitation intensity is about 30 W/cm². [Publ. VI]

nificantly. Figs. 5.6(a), (b) and (c) show the comparison of the $[110]$ cross-sectional profiles of a typical QR grown at $T_g = 500$ °C but annealed at $T_a = 500$ °C, $T_a = 550$ °C, and $T_a = 570$ °C, respectively. Fig. 5.6(d) shows the temperature sequences of the QR fabrication in Fig. 5.6(a), (b) and (c). Fig. 5.6(e) shows a 3D AFM image of QRs grown at $T_g = 500$ °C and annealed at $T_a = 570$ °C. It can be seen that the camel-hump like shape disappears and the QRs are less elongated when annealed at higher temperature. Compared to the QRs annealed at 500 °C, the height of the QR rim in $[110]$ direction is decreased from 11 nm to 5 nm and to 3 nm when the annealing temperature is 550 °C and 570 °C, respectively. The diameter of the QR measured from the outer edge is not affected. In $[1\bar{1}0]$ direction, on the other hand, the height of the rim is almost the same (~ 3 nm) in these three cases and the lateral dimension is closer to that of $[110]$ direction when the annealing temperature is higher. It indicates that the diffusion rate of the indium atoms depends not only on the crystal direction but also on the temperature. The diffusion rate of the indium atoms is more isotropic at higher temperatures. Furthermore, it seems that the void is somewhat deeper at higher annealing temperatures, which might be caused by the removal of the intermixed lower island interface.

Low temperature PL spectra from the buried InAs islands (QDs) and QRs are shown in Fig. 5.7(a). InAs islands were formed by depositing a nominal 1.7-ML-thick InAs layer at $T_a = 550$ °C and QRs were formed from these InAs islands by using a 2-nm-thick partial capping layer and annealing for 60 s at $T_a = T_g = 550$ °C. Both samples were covered with a 50-nm-thick GaAs barrier layer. PL peaks from the QDs and the QRs were observed at 1.04 eV and 1.22 eV with the full width at half

maximum (FWHM) of 87 meV and 75 meV, respectively. The PL peak of the QRs is blue-shifted by about 180 meV with respect to the QD peak.

Fig. 5.7(b) shows low-temperature PL spectra of the QRs described in Fig. 5.6. When T_a is increased from 500 °C to 570 °C in QRs grown at $T_g = 500$ °C, the PL emission peak from the QRs is blue-shifted from 1.21 eV to 1.24 eV. This indicates that at higher annealing temperatures more indium atoms have diffused away from the islands so that the In composition in the InGaAs rim becomes smaller. Also, the smaller height of the ring (as seen from Fig. 5.6) can affect the PL peak energy via the more pronounced quantization of the energy levels. Moreover, it was observed that the PL intensity of the QRs with $T_a = 570$ °C is more than ten times higher compared to that of QRs with $T_a = 500$ °C. Higher PL intensity is assumed to be caused by the higher crystal quality of the GaAs barrier layer grown at higher growth temperatures [127].

6 Summary

The aim of this work was twofold: (i) to find out the effective methods and materials for passivation of the GaAs surface by using in-situ epitaxial growth and ex-situ deposition techniques, and (ii) to characterize InAs/GaAs quantum dot and quantum ring structures fabricated by MOVPE, i.e., study the effect of growth conditions on surface morphology and optical properties of the dots and rings.

The study of GaAs surface passivation was carried out by investigating the optical properties of passivated InGaAs NSQW structures due to their sensitivity to surface states. NSQW structures and *in-situ* passivation layers were fabricated by MOVPE. Ultra-thin InP, GaP, GaN layers were grown on top of the NSQW structure as the passivation layer. As–P and As–N exchange on the GaAs surface were also applied for passivation. In all the passivation methods, the optical properties of the NSQWs were significantly improved: the PL intensity was enhanced at best by a factor of more than two orders of magnitude, the carrier lifetimes increased notably, and the surface built-in electric fields were reduced remarkably. The study of time durability of the passivation after keeping the passivated samples for a long time in air ambient showed that those passivation methods protect the samples against oxidation while the unpassivated samples degrade severely. The passivation effects of these materials were also studied by using NSQWs fabricated on (110)-oriented GaAs substrates. The suitability of atomic layer deposited titanium nitride layer on the GaAs surface as an *ex-situ* passivation layer was also investigated. Although the enhancement factor of the PL intensity is smaller than that obtained by *in-situ* methods, smooth surface morphology and a notable extension of carrier the lifetime were observed.

Self-assembled InAs islands with an average areal density of 10^9 cm^{-2} were obtained on a GaAs (110) substrate at 400 °C using a thin InGaAs strain reducing layer. AFM and low temperature PL measurements were used to study the island properties. Effects of growth conditions on island properties were studied and compared to that of on GaAs (100) substrate. The results show that the substrate orientation plays important role in 3D island formation and results in different properties of the islands grown on differently oriented substrates. Transformation of InAs islands into rings was realized by partially capping the InAs islands and annealing under tertiarybutylarsine (TBAs) flow on GaAs (100) substrate. QRs with an areal density of $10^7\text{--}10^9 \text{ cm}^{-2}$ were obtained at 500–600 °C. Ring transformation significantly affects the morphological and optical properties of the islands. The optimum values

for the annealing time and the partial capping layer thickness were found to be 60–120 s and 0.5–2.0 nm, respectively. The geometric shape of the rings is elongated in [110] direction due to the anisotropy of the diffusion rate of the indium atoms. However, this elongation is reduced in the QRs annealed at higher temperatures. Low-temperature PL peak at 1.22 eV is obtained from the buried QRs grown at 550 °C. A blue shift of the PL peak is observed when the annealing temperature is increased.

In this work, only the optical properties of the samples are used for investigating the GaAs surface passivation effects. Although improved PL, TRPL, PR measurement results were obtained from passivated samples, further studies of the structural and electrical properties of the surfaces of the passivated samples are essential in order to understand the mechanism responsible for the passivation. Since the thickness of the passivation layer is very thin and growth temperature is quite high, there are difficulties to apply the MOVPE passivation methods on devices. However, one can try to design a device structure where the passivation layer on top of the structure could be useful. Another approach is to utilize low-temperature ALD growth to passivate the surfaces of the devices. Moreover, some other optical characterization methods, i.e, reflection anisotropy spectroscopy (RAS), x-ray photoelectron spectroscopy (XPS) and photoemission spectroscopy (PES) are also powerful tools for surface characterization.

Since the transformation of QRs happens during the annealing partially capped islands, it would be very helpful to fully understand the transformation process if *in-situ* monitoring techniques are applied. By real-time *in-situ* techniques, such as, spectral reflectance (SR), laser light scattering (LLS), and RAS measurements, it could be possible to observe the surface morphology at every step of ring transformation. Furthermore, transmission electron microscopy (TEM) will be more helpful to study the overgrown QDs and QRs.

References

- [1] P. Bhattacharya, *Semiconductor Optoelectronic Devices* (Prentice-Hall, Inc., 1997), 2nd ed.
- [2] R. N. Hall, G. E. Fenner, J. D. Kingsley, T. J. Soltys and R. O. Carlson, *Phys. Rev. Lett.* **9**, 366 (1962).
- [3] J. B. Gunn, *Solid State Commun.* **1**, 88 (1963).
- [4] M. R. Lorenz, G. D. Pettit and R. C. Taylor, *Phys. Rev.* **171**, 876 (1968).
- [5] R. A. Logan, H. G. White and W. Wiegmann, *Appl. Phys. Lett.* **13**, 139 (1968).
- [6] H. Amano, M. Kito, K. Hiramatsu and I. Akasaki, *Jpn. J. Appl. Phys.* **28**, L2112 (1989).
- [7] S. Nakamura, T. Mukai, M. Senoh and N. Iwasa, *Jpn. J. Appl. Phys.* **31**, L139 (1992).
- [8] S. Nakamura, M. Senoh, N. Iwasa, S. Nagahama, T. Yamada and T. Mukai, *Jpn. J. Appl. Phys.* **34**, L1332 (1995).
- [9] S. Nakamura, M. Senoh, N. Iwasa and S. Nagahama, *Jpn. J. Appl. Phys.* **34**, L797 (1995).
- [10] J. Riikonen, Ph.D. thesis, Helsinki University of Technology (2006).
- [11] A. A. Allerman, R. M. Biefeld and S. R. Kurtz, *Appl. Phys. Lett.* **69**, 465 (1996).
- [12] J. L. Johnson, L. A. Samoska, A. C. Gossard, J. L. Merz, M. D. Jack, G. R. Chapman, B. A. Baumgratz, K. Kosai and S. M. Johnson, *J. Appl. Phys.* **80**, 1117 (1996).
- [13] T. Mukai, D. Morita and S. Nakamura, *J. Cryst. Growth* **189/190**, 778 (1998).
- [14] F. C. Frank and J. H. van der Merwe, *Proc. Roy. Soc. London* **A198**, 216 (1949).
- [15] M. Volmer and A. Weber, *Z. Physik. Chem.* **119**, 277 (1926).
- [16] I. N. Stranski and L. Krastanow, *Sitz. Ber. Akad. Wiss., Math.-naturwiss. Kl.* **Iib 146**, 797 (1938).
- [17] D. J. Eaglesham and M. Cerullo, *Phys. Rev. Lett.* **64**, 1943 (1990).

- [18] S. Guha, A. Madhukar and K. C. Rajkumar, Appl. Phys. Lett. **57**, 2110 (1990).
- [19] T. R. Ramachandran, R. Heitz, P. Chen and A. Madhukar, Appl. Phys. Lett. **70**, 640 (1997).
- [20] R. Nötzel, J. Temmyo and T. Tamamura, Nature **369**, 131 (1994).
- [21] S. Sopanen, H. Lipsanen and J. Ahopelto, Appl. Phys. Lett. **67**, 3768 (1995).
- [22] A. Ponchet, A. Le Corre, H. L'Haridon, B. Lambert and S. Salaün, Appl. Phys. Lett. **67**, 1850 (1995).
- [23] F. Hatami, N. N. Ledentsov, M. Grundmann, J. Böhrer, F. Heinrichsdorff, M. Beer, D. Bimberg, S. S. Ruvimov, P. Werner, U. Gösele, J. Heydenreich, U. Richter, S. V. Ivanov, B. Y. Meltser, P. S. Kop'ev and Z. I. Alferov, Appl. Phys. Lett. **67**, 656 (1995).
- [24] W. Mönch, *Semiconductor Surfaces and Interfaces*, (Springer, 1995), 2nd ed.
- [25] C. Kittel, *Introduction to solid state physics*, (John Wiley & Sons, Inc, 2005), 8th ed.
- [26] K. Oura, V. G. Lifshits, A. A. Saranin, A. V. Zotov and M. Katayama, *Surface Science: An introduction*, (Springer, 2003).
- [27] P. Y. Yu and M. Cardona, *Fundamentals of Semiconductors: Physics and Materials properties*, (Springer, 2003), 2nd ed.
- [28] P. H. Holloway and G. E. McGuire, *Handbooks of compound semiconductors: Growth, Processing, Characterization, and Devices*, (William Andrew Publishing/Noyes, 1995).
- [29] V. M. Botnaryuk, Y. V. Zhilyaev and E. V. Konenkova, Semiconductor **33**, 662 (1999).
- [30] N. G. Wright, C. M. Johnson and A. G. O'Neill, IEEE, ISPSD '97. p. 141 (1997).
- [31] K. P. Hsueh, H. T. Hsu, C. H. Wu and Y. M. Hsin, Semicond. Sci. Technol. **19**, L118 (2004).
- [32] G. Wang, K. Ohtsuka, T. Soga, J. T. and M. Umeno, Jpn. J. Appl. Phys. **38**, 3504 (1999).
- [33] T. Ohno, Phys. Rev. B **44**, 6306 (1991).
- [34] T. Ohno and K. Shiraishi, Phys. Rev. B **42**, 11194 (1990).
- [35] V. N. Bessolov, M. V. Lebedev, N. M. Friedrich and D. R. T. Zahn, Semicond. Sci. Technol. **13**, 611 (1998).

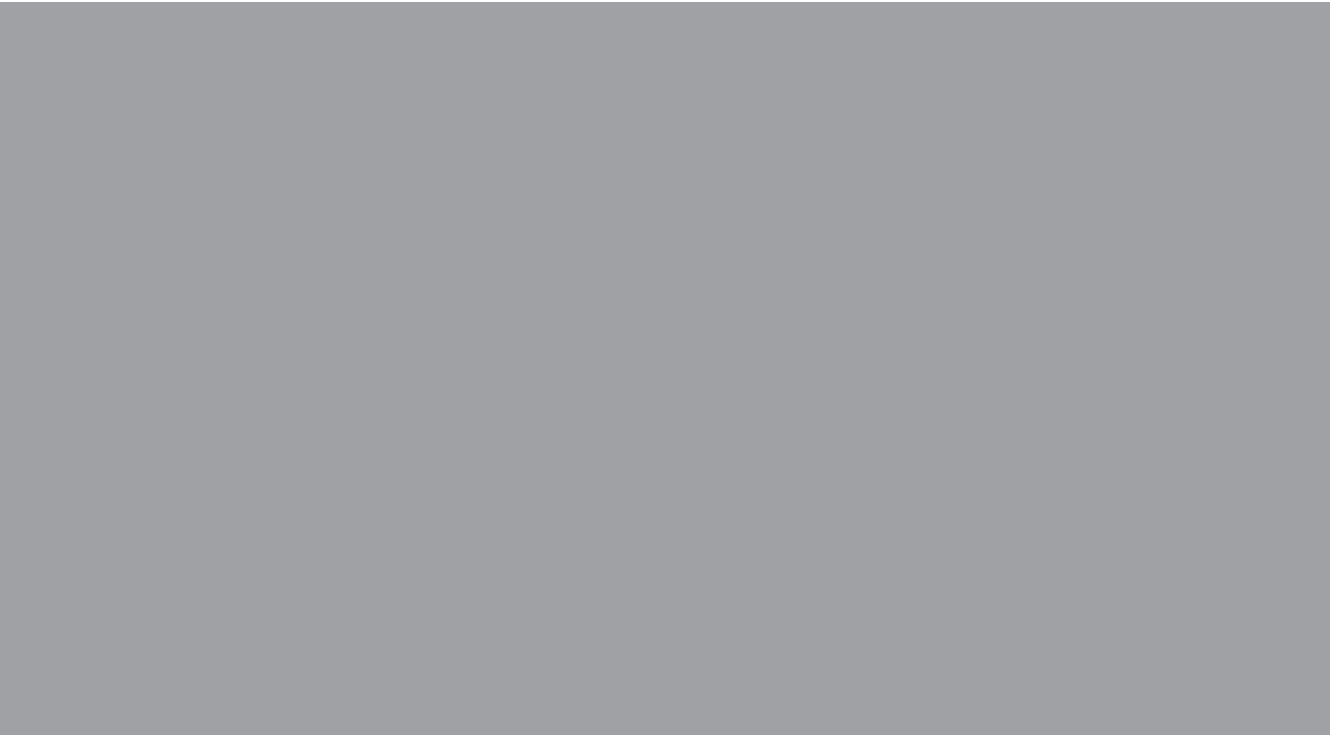
- [36] G. Eftekhari, *Vacuum* **67**, 81 (2002).
- [37] P. Viktorovitch, M. Gendry, S. K. Krawczyk, F. Krafft, A. P., A. Bekkaoui and Y. Monteil, *Appl. Phys. Lett.* **58**, 2387 (1991).
- [38] D. A. Harrison, R. Arès, S. P. Watkins, M. L. W. Thewalt, C. R. Bolognesi, D. J. S. Beckett and A. J. Spring Thorpe, *Appl. Phys. Lett.* **70**, 3275 (1997).
- [39] R. Beaudry, S. P. Watkins, X. Xu and P. Yeo, *J. Appl. Phys.* **87**, 7838 (2000).
- [40] R. Pal, S. P. Shivaprasad, X. Aparna and P. Chakraborty, *Appl. Surf. Sci.* **245**, 196 (2005).
- [41] T. Sugino, H. Ninomiya, J. Shirafuji and K. Matsuda, *Appl. Phys. Lett.* **72**, 1472 (1998).
- [42] B. I. Bednyi and N. V. Baidus, *Semiconductors* **30**, 132 (1996).
- [43] G. Bruno, *Appl. Surf. Sci.* **235**, 239 (2004).
- [44] S. Anantathanasarn and H. Hasegawa, *Appl. Surf. Sci.* **190**, 343 (2002).
- [45] C. J. Sandroff, R. N. Nottenburg, J. C. Bischoff and R. Bhat, *Appl. Phys. Lett.* **51**, 33 (1987).
- [46] H. H. Lee, R. J. Racicot and S. H. Lee, *Appl. Phys. Lett.* **54**, 752 (1989).
- [47] G. Wang, T. Ogawa, M. Umeno, T. Soga and J. T., *Appl. Phys. Lett.* **76**, 730 (2000).
- [48] R. Mosca, E. Gombia, A. Passaseo, V. Tasco, M. Peroni and P. Romanini, *Superlattices and Microstructures* **36**, 425 (2004).
- [49] T. Hashizume, K. Ikeya, M. Mutoh and H. Hasegawa, *Appl. Surf. Sci.* **123/124**, 599 (1998).
- [50] R. Singh and H. Hartnagel, *J. Phys. D: Appl. Phys.* **8**, L42 (1975).
- [51] M. Hong, M. Passlack, J. P. Mannaerts, T. D. Harris, M. L. Schnoes, R. L. Opila and H. W. Krautter, *Solid-State Electronics* **41**, 643 (1997).
- [52] T. S. Shamirzaev, K. S. Zhuravlev, A. Y. Kobitski, H. P. Wagner and D. R. T. Zahn, *Physica B* **308-310**, 761 (2001).
- [53] N. Shiozaki, S. Anantathanasarn, T. Sato, T. Hashizume and H. Hasegawa, *Appl. Surf. Sci.* **244**, 71 (2004).
- [54] Y. Wada and K. Wada, *Appl. Phys. Lett.* **63**, 379 (1993).
- [55] H. Lipsanen, M. Sopanen, M. Taskinen and J. Tulkki, *Appl. Phys. Lett.* **68**, 2216 (1996).

- [56] J. Riikonen, J. Sormunen, H. Koskenvaara, M. Mattila and M. Sopanen, *J. Cryst. Growth* **272**, 621 (2004).
- [57] J. Sormunen, Ph.D. thesis, Helsinki University of Technology (2006).
- [58] J. M. Llorens, C. Trallero-Giner, A. García-Cristóbal and A. Cantarero, *Microelectron. J.* **33**, 355 (2002).
- [59] I. Filikhin, V. M. Suslov and B. Vlahovic, *Physica E* **33**, 349 (2006).
- [60] A. O. Govorov, S. E. Ulloa, K. Karrai and R. J. Warburton, *Phys. Rev. B* **66**, 081309 (2002).
- [61] R. J. Warburton, C. Schäfflein, D. Haft, F. Bickel, A. Lorke, K. Karrai, J. M. Garcia, W. Schoenfeld and P. M. Petroff, *Physica E* **9**, 124 (2001).
- [62] D. Haft, C. Schulhauser, A. O. Govorov, R. J. Warburton, K. Karrai, J. M. Garcia, W. Schoenfeld and P. M. Petroff, *Physica E* **13**, 165 (2002).
- [63] O. Voskoboynikov and C. P. Lee, *Physica E* **20**, 278 (2004).
- [64] J. Planelles, W. Jaskólski and J. I. Aliaga, *Phys. Rev. B* **65**, 033306 (2001).
- [65] A. Lorke, R. J. Luyken, A. O. Govorov, J. P. Kotthaus, J. M. García and P. M. Petroff, *Phys. Rev. Lett.* **84**, 2223 (2000).
- [66] F. Suárez, D. Granados and J. M. García, *Nanotechnology* **15**, S126 (2004).
- [67] Y. Aharonov and D. Bohm, *Phys. Rev.* **115**, 485 (1959).
- [68] T. Chakraborty and P. Pietiläinen, *Phys. Rev. B* **50**, 8460 (1994).
- [69] R. A. Römer and M. E. Raikh, *physica status solidi (b)* **221**, 535 (2000).
- [70] U. F. Keyser, C. Fühner, S. Borck, R. J. Haug, M. Bichler, G. Abstreiter and W. Wegscheider, *Phys. Rev. Lett.* **90**, 196601 (2003).
- [71] J. M. García, G. Medeiros-Ribeiro, K. Schmidt, T. Ngo, J. L. Feng, A. Lorke, J. Kotthaus and P. M. Petroff, *Appl. Phys. Lett.* **71**, 2014 (1997).
- [72] K. Takehana, F. Pulizzi, A. Patane, M. Henini, P. C. Main, L. Eaves, D. Granados and J. M. García, *J. Cryst. Growth* **251**, 155 (2003).
- [73] D. Granados and J. M. García, *J. Cryst. Growth* **251**, 213 (2003).
- [74] D. Granados and J. M. García, *Appl. Phys. Lett.* **82**, 2401 (2003).
- [75] B. C. Lee and C. P. Lee, *Nanotechnology* **15**, 848 (2004).
- [76] T. Raz, D. Ritter and G. Bahir, *Appl. Phys. Lett.* **82**, 1706 (2003).

- [77] S. Kobayashi, C. Jiang, T. Kawazu and H. Sakaki, *Jpn. J. Appl. Phys.* **43**, L662 (2004).
- [78] P. J. Poole, P. L. Williams, J. Lefebvre and S. Moisa, *J. Cryst. Growth* **257**, 89 (2003).
- [79] J. Sormunen, J. Riikonen, M. Mattila, J. Tiilikainen, M. Sopanen and H. Lipsanen, *Nano Lett.* **5**, 1541 (2005).
- [80] Z. Gong, Z. C. Niu, S. S. Huang, Z. D. Fang, B. Q. Sun and J. B. Xia, *Appl. Phys. Lett.* **87**, 093116 (2005).
- [81] F. Ding, L. Wang, S. Kiravittaya, E. Müller, A. Rastelli and O. G. Schmidt, *Appl. Phys. Lett.* **90**, 173104 (2007).
- [82] A. Lorke, R. J. Luyken, J. M. García and P. M. Petroff, *Jpn. J. Appl. Phys.* **40**, 1857 (2001).
- [83] A. Lorke, R. Blossey, J. M. García, M. Bichler and G. Abstreiter, *Mater. Sci. Eng. B* **88**, 225 (2002).
- [84] R. Blossey and A. Lorke, *Phys. Rev. E* **65**, 021603 (2002).
- [85] M. Manasevit and W. Simpson, *J. Electrochem. Soc.* **116**, 1725 (1969).
- [86] M. E. Heimbuch, A. L. Holmes, Jr., C. M. Reaves, M. P. Mack, S. P. DenBaars and L. A. Coldren, *J. Electron Mater.* **23**, 87 (1994).
- [87] T. Suntola and J. Antson, U.S. Patent p. 4058430 (1977).
- [88] R. L. Puurunen, *J. Appl. Phys.* **97**, 121301 (2005).
- [89] L. Niinistö, J. Päiväsaari, J. Niinistö, M. Putkonen and M. Nieminen, *phys. stat. sol. (a)* **201**, 1443 (2004).
- [90] G. Binning, C. F. Quate and C. Gerbe, *Phys. Rev. Lett.* **56**, 930 (1986).
- [91] S. Perkowitz, *Optical characterization of Semiconductors: Infrared, Raman, and Photoluminescence Spectroscopy* (Academic press, Inc., 1993).
- [92] C. R. Brundle, C. A. Evans, Jr. and S. Wilson, *Encyclopedia of Materials Characterization – Surfaces, Interfaces, Thin Films* (Butterworth-Heinemann, 1992).
- [93] H. Shen and M. Dutta, *J. Appl. Phys.* **78**, 2151 (1995).
- [94] X. Yin, H.-M. Chen, F. H. Pollak, Y. Chan and P. A. Montano, *J. Vac. Sci. Technol. A* **10**, 131 (1992).
- [95] J. M. Moison, K. Elcess, F. Houzay, J. Y. Marzin, J. M. Gérard, F. Barthe and M. Bensoussan, *Phys. Rev. B* **41**, 12945 (1990).

- [96] H. Yang, O. Brandt, A. Trampert and K. H. Ploog, *Appl. Surf. Sci.* **104/105**, 461 (1996).
- [97] J. Sormunen, J. Toivonen, M. Sopanen and H. Lipsanen, *Appl. Surf. Sci.* **222**, 286 (2004).
- [98] E. Yablonovitch, B. J. Skromme, R. Bhat, J. P. Harbison and T. J. Gmitter, *Appl. Phys. Lett.* **54**, 555 (1989).
- [99] H. X. Jiang, E. X. Ping, P. Zhou and J. Y. Lin, *Phys. Rev. B* **41**, 12949 (1990).
- [100] J. Dreybrodt, F. Daiminger, J. P. Reithmaier and A. Forchel, *Phys. Rev. B* **51**, 4657 (1995).
- [101] C. Symonds, J. Mangeney, G. Saint-Girons and I. Sagnes, *Appl. Phys. Lett.* **87**, 012107 (2005).
- [102] M. Stobbe, R. Redmer and W. Schattke, *Phys. Rev. B* **49**, 4494 (1994).
- [103] H. Kroemer, K. J. Polasko and S. C. Wright, *Appl. Phys. Lett.* **36**, 763 (1980).
- [104] N. K. Dutta, W. S. Hobson, G. J. Zydzi, J. F. de Jong, P. Parayanthal, M. Passlack and U. K. Chakrabarti, *IEE Electronics Letters* **33**, 213 (1997).
- [105] P. Ressel, G. Erbert, U. Zeimer, K. Hausler, G. Beister, B. Sumpf, A. Klehr and G. Trankle, *IEEE Photonics Technology Letters* **17**, 962 (2005).
- [106] M. Lopez, Y. Takano, K. Pak and H. Yonezu, *Appl. Phys. Lett.* **58**, 580 (1990).
- [107] R. Hey, A. Trampert and P. Santos, *Phys. Stat. Sol.(c)* **3**, 651 (2006).
- [108] L. T. P. Allen, E. R. Weber, J. Washburn, Y. C. Pao and A. G. Elliot, *J. Cryst. Growth* **87**, 193 (1988).
- [109] D. M. Holmes, J. G. Belk, J. L. Sudijono, J. H. Neave, T. S. Jones and B. A. Joyce, *Surface Science* **341**, 133 (1995).
- [110] J. M. McCoy and J. P. LaFemina, *Phys. Rev. B* **54**, 14511 (1996).
- [111] Z. W. Deng, R. W. M. Kwok, W. M. Lau and L. L. Cao, *Appl. Sur. Sci.* **158**, 58 (2000).
- [112] Y. Wada and K. Wada, *J. Vac. Sci. Technol. B* **11(4)**, 1598 (1993).
- [113] Y. Arakawa and H. Sakaki, *Appl. Phys. Lett.* **40**, 939 (1982).
- [114] L. Golstein, F. Glas, J. Y. Marzin, M. N. Charasse and G. Le Roux, *Appl. Phys. Lett.* **47**, 1099 (1985).

- [115] X. Zhang, D. W. Pashley, J. H. Neave, P. N. Fawcett, J. Zhang and B. A. Joyce, *J. Cryst. Growth* **132**, 331 (1993).
- [116] D. Wasserman and S. A. Lyon, *Appl. Phys. Lett.* **85**, 5352 (2004).
- [117] M. Blumin, H. E. Ruda, I. G. Savelyev, A. Shik and H. Wang, *J. Appl. Phys.* **99**, 093518 (2006).
- [118] D. Schuh, J. Bauer, E. Uccelli, R. Schulz, A. Kress, F. Hofbauer, J. J. Finley and G. Abstreiter, *Physica E* **26**, 72 (2005).
- [119] C. X. Cui, Y. H. Chen, C. L. Zhang, P. R. Jin, G. X. Shi, C. Zhao, B. Xu and Z. G. Wang, *Physica E* **28**, 537 (2005).
- [120] M. A. Cusack, P. R. Briddon and M. Jaros, *Phys. Rev. B* **56**, 4047 (1997).
- [121] I. Daruka and A. Barabási, *Phys. Rev. Lett.* **79**, 3708 (1997).
- [122] Y. H. Chen, X. L. Ye and Z. G. Wang, *Nanoscale Res. Lett.* **1**, 79 (2006).
- [123] L. Nasi, C. Bocchi, F. Germini, M. Prezioso, R. Gombia, E. Mosca, P. Frigeri, G. Trevisi, L. Seravalli and S. Franchi, *J. Mater. Sci: Mater Electron* (in press, 2008).
- [124] D. Leonard, K. Pond and P. M. Petroff, *Phys. Rev. B* **50**, 11687 (1994).
- [125] D. Leonard, M. Krishnamurthy, C. M. Reaves, S. P. Denbaars and P. M. Petroff, *Appl. Phys. Lett.* **63**, 3203 (1993).
- [126] G. M. Guryanov, G. E. Cirlin, V. N. Petrov, N. K. Polyakov, A. O. Golubok, S. Y. Tipishev, V. B. Gubanov, Y. B. Samsonenko, N. N. Ledentsov, V. A. Shchukin, M. Grundmann, D. Bimberg and Z. I. Alferov, *Surf Sci.* **352-354**, 651 (1996).
- [127] R. Ohtsubo and K. Yamaguchi, *phys. stat. sol. (c)* **0**, 939 (2003).



ISBN 978-951-22-9614-9
ISBN 978-951-22-9615-6 (PDF)
ISSN 1795-2239
ISSN 1795-4584 (PDF)